

ARTICLE TYPE

Multigrid reduction-in-time convergence for advection problems: A Fourier analysis perspective[†]

H. De Sterck¹ | S. Friedhoff² | O. A. Krzysik^{*1} | S. P. MacLachlan³

¹Department of Applied Mathematics,
University of Waterloo, ON, Canada

²Department of Mathematics, Bergische
Universität Wuppertal, Germany

³Department of Mathematics and Statistics, ,
Memorial University of Newfoundland, ,
NL, Canada

Correspondence

Email: okrzysik@uwaterloo.ca

Abstract

A long-standing issue in the parallel-in-time community is the poor convergence of standard iterative parallel-in-time methods for hyperbolic partial differential equations (PDEs), and for advection-dominated PDEs more broadly. Here, a local Fourier analysis (LFA) convergence theory is derived for the two-level variant of the iterative parallel-in-time method of multigrid reduction-in-time (MGRIT). This closed-form theory allows for new insights into the poor convergence of MGRIT for advection-dominated PDEs when using the standard approach of rediscrctizing the fine-grid problem on the coarse grid. Specifically, we show that this poor convergence arises, at least in part, from inadequate coarse-grid correction of certain smooth Fourier modes known as characteristic components, which was previously identified as causing poor convergence of classical spatial multigrid on steady-state advection-dominated PDEs. We apply this convergence theory to show that, for certain semi-Lagrangian discretizations of advection problems, MGRIT convergence using rediscrctized coarse-grid operators cannot be robust with respect to CFL number or coarsening factor. A consequence of this analysis is that techniques developed for improving convergence in the spatial multigrid context can be re-purposed in the MGRIT context to develop more robust parallel-in-time solvers. This strategy has been used in recent work to great effect; here, we provide further theoretical evidence supporting the effectiveness of this approach.

KEYWORDS:

Parallel-in-time methods, MGRIT, Parareal, advection equations, local Fourier analysis

1 | INTRODUCTION

Parallel-in-time methods for the solution of initial-value, time-dependent partial differential equations (PDEs) have seen an increase in both popularity and relevance over the past two decades, with the advancement of massively parallel computers. Thorough reviews of the parallel-in-time field are given by Gander¹ and, Ong & Schroder.² In this paper, we study the convergence of the multigrid reduction-in-time (MGRIT) algorithm,³ which, as its name implies, achieves temporal parallelism by deploying multigrid techniques in the temporal direction. Our work also applies to the well-known Parareal method,⁴ since the two-grid variant of MGRIT is the same as Parareal for certain choices of algorithmic parameters.

[†]This work was supported in part by NSERC of Canada. The work of the third author was partially supported by an Australian Government Research Training Program Scholarship.

A long-standing issue in the parallel-in-time field is the development of efficient solvers for hyperbolic PDEs, and for advection-dominated PDEs more broadly. It is well-documented that the convergence of MGRIT and Parareal is typically poor for advection-dominated problems.^{5–21} In fact, slow and non-robust convergence of these methods for advection-dominated problems has, for the most part, precluded any significant parallel speed-ups over sequential time-stepping. This is in stark contrast to diffusion-dominated PDEs, for which convergence is typically fast, and is typically robust with respect to PDE, discretization, and algorithmic parameters, resulting in substantial speed-ups over time-stepping.

While our focus in this paper is on multigrid-in-time methods, we note that other parallel-in-time strategies have been developed for advective and wave-propagation problems that do not appear to suffer from the same poor convergence as Parareal and MGRIT.^{22–26} In particular, the referenced algorithms rely (in one form or another) on diagonalizing the discretized problem in the time direction and then solving in parallel a set of decoupled linear systems, a technique introduced by Maday and Rønquist.²⁷

A large number of convergence analyses for MGRIT and Parareal have been developed,^{8–10, 18, 28–32}, with several paying particular attention to advection-related problems.^{7, 9, 10, 18, 28} Yet, there is no widely accepted explanation for what fundamentally makes the parallel-in-time solution of these problems so difficult. In De Sterck et al.,⁷ informed by the convergence theory of Dobrev et al.,⁸ we developed a heuristic optimization strategy for building coarse-grid operators. While yielding previously unattained convergence rates, our coarse-grid operators were limited to constant-wave-speed advection problems, relying on prohibitively expensive computation to determine these operators. So, while there are many MGRIT and Parareal convergence analyses, none so far appear to have inspired the development of efficient and practical solvers for advection-dominated PDEs.

Here, we analyze the convergence of two-level MGRIT through the lens of local Fourier analysis (LFA). Originally proposed by Brandt,³³ LFA is a predictive tool for studying the convergence behaviour of multigrid methods, and is the most widely used tool for doing so.^{34–39} LFA has been used previously to investigate MGRIT convergence,^{28, 29} as well as other multigrid-in-time methods.^{36, 40–42} A particular novelty of our LFA theory is that it is presented in closed form, which offers significantly more insight than previous efforts, such as in References 28, 29. That is, we provide analytical expressions for the LFA predictions of the norm and spectral radius of the error propagation operator, rather than arriving at them through semi-analytical means (i.e., with some numerical assistance). Such closed-form LFA results are well-known for some simple cases (e.g., optimizing the relaxation parameter in weighted Jacobi), but are not always attainable, particularly when applying the method to complicated PDEs or algorithms.⁴³ As another example, even closed-form convergence factors for MGRIT applied to discretizations of linear advection are not currently known.

Our LFA theory yields results consistent with the prior MGRIT analyses of References 8, 31, 32, 44, which were derived using different analysis tools. Thus, in this sense our LFA does not yield “new” final convergence bounds. However, the fact that we have closed-form convergence results in temporal Fourier space allows us to draw important new connections between the convergence issues of MGRIT and those of classical spatial multigrid methods in a way that these existing theories cannot. Specifically, it is widely known for spatial multigrid methods that poor coarse-grid correction of certain smooth Fourier modes known as *characteristic components* leads to convergence issues for steady-state advection-dominated problems.^{34, 37, 39, 45–49} Here, we establish that this is the case for MGRIT also, with poor convergence due, at least in part, to an inadequate coarse-grid correction of smooth space-time characteristic components, which was something initially suggested to us by the author of Reference 39.

This new connection suggests that MGRIT solvers with increased robustness could be developed by generalizing the fixes proposed in the steady-state setting. In fact, in a sequence of recent papers,^{50–52} we have leveraged this connection to develop fast MGRIT-based solvers for hyperbolic PDEs that far outperform those based on standard rediscritization or direct discretization techniques, even including for nonlinear hyperbolic PDEs with shocks.⁵² Underlying each of these solvers is the use of an idea developed by Yavneh³⁹ in the steady-state case of increasing the accuracy of the coarse-grid operator relative to the fine-grid operator. By formally establishing this link with spatial multigrid methods, this paper provides the theoretical foundations for the advancements made in References 50–52.

The remainder of this paper is organised as follows. An algorithmic description of MGRIT and key assumptions are presented in Section 2. Section 3 describes the error propagation operator of the MGRIT algorithm. The LFA convergence theory is presented in Section 4. A short comparison to related literature is given in Section 5. In Section 6, the LFA theory is used to describe the link between convergence of MGRIT and spatial multigrid methods, and this is applied to analyze MGRIT convergence for a class of semi-Lagrangian discretizations of linear advection problems. Concluding remarks are given in Section 7.

2 | PRELIMINARIES

Section 2.1 provides a brief overview of the MGRIT algorithm as it applies to linear problems, and Section 2.2 describes some key assumptions and notation used in our analysis.

2.1 | MGRIT

Consider the linear, initial-value problem (IVP) $\frac{\partial u}{\partial t} = \mathcal{L}(u) + f$ with $u(x, 0) = u_0(x)$. Suppose this problem is fully discretized in space and time using a one-step method to yield the discrete equations

$$\mathbf{u}_{n+1} = \Phi \mathbf{u}_n + \mathbf{g}_{n+1}, \quad n = 0, 1, \dots, n_t - 2, \quad (1)$$

supplemented with the initial data $\mathbf{u}_0 \in \mathbb{R}^{n_x}$, where \mathbf{u}_n is the spatially discrete approximation to $u(x, t_n)$. In (1), $\Phi \in \mathbb{R}^{n_x \times n_x}$ is the *time-stepping operator* that, in this work, we assume is linear, and is time independent. Discretized systems as in (1) arise in several contexts, including the method-of-lines discretization process, for arbitrary spatial discretization of $\mathcal{L}(u)$ and one-step (but, possibly, multi-stage) discretization of the time derivative. The vector $\mathbf{g}_{n+1} \in \mathbb{R}^{n_x}$ contains solution-independent information pertaining to spatial boundary conditions and source terms. The system (1) is naturally solved by sequential time-stepping: Computing \mathbf{u}_1 from \mathbf{u}_0 , then \mathbf{u}_2 from \mathbf{u}_1 , and so on. By contrast, a parallel-in-time method seeks the solution of (1) over all values of n in parallel. With this in mind, it is convenient to assemble the equations in (1) into the global linear system

$$A_0 \mathbf{u} := \begin{bmatrix} I & & & \\ -\Phi & I & & \\ & \ddots & \ddots & \\ & & -\Phi & I \end{bmatrix} \begin{bmatrix} \mathbf{u}_0 \\ \mathbf{u}_1 \\ \vdots \\ \mathbf{u}_{n_t-1} \end{bmatrix} = \begin{bmatrix} \mathbf{u}_0 \\ \mathbf{g}_1 \\ \vdots \\ \mathbf{g}_{n_t-1} \end{bmatrix} =: \mathbf{b}. \quad (2)$$

MGRIT³ iteratively computes the solution of (2) by employing multigrid reduction techniques in the time direction. To this end, let us associate with (1) a grid of n_t equispaced points in time: $0 = t_0 < t_1 < \dots < t_{n_t-1} = T$, with $t_n = n\delta t$ and time step δt . Let these time points constitute a “fine grid,” and let a coarsening factor $m \in \mathbb{N}$ induce a “coarse grid,” consisting of every m th fine-grid point. The set of points appearing exclusively on the fine grid are called F-points, while those shared by both fine and coarse grids are C-points. For simplicity, we assume that t_0 is a C-point, and that n_t is divisible by m .

A single MGRIT iteration on (2) consists of pre-relaxation, a coarse-grid correction, and then post-relaxation, which we now detail. Suppose we have an approximation $\mathbf{w} \approx \mathbf{u}$, with $\mathbf{r} = \mathbf{b} - A_0 \mathbf{w}$ denoting its algebraic residual. Pre- and post-relaxation on $A_0 \mathbf{w} \approx \mathbf{b}$ are built by composing F- and C-relaxation sweeps, which update \mathbf{w} to set the resulting \mathbf{r} to zero at F- and C-points, respectively. F-relaxation can be thought of as time-stepping \mathbf{w} from each C-point across the interval of $m - 1$ F-points that follow it, called the CF-interval in the following, and C-relaxation can be thought of as time-stepping \mathbf{w} from the last F-point in each CF-interval to its neighbouring C-point in the next CF-interval. F- and C-relaxations are local operations and are, therefore, highly parallelizable. In this work, post-relaxation is fixed as a single F-relaxation, while we denote pre-relaxation by $F(\text{CF})^\nu$, $\nu \in \mathbb{N}_0$, meaning a single F-relaxation followed by ν sweeps of CF-relaxation (each composed of a sweep of C-relaxation followed by one of F-relaxation). Common choices are $\nu = 0$ or 1 , written as F- and FCF-relaxation, respectively, but larger values of ν can also be considered.^{30–32}

After pre-relaxation, the coarse-grid correction step solves the reduced system $A_1 \mathbf{e}_\Delta = \mathbf{r}_\Delta$, which has a factor of m fewer time points. Here, \mathbf{r}_Δ is the fine-grid residual vector injected to the C-points,

$$A_1 := \begin{bmatrix} I & & & \\ -\Psi & I & & \\ & \ddots & \ddots & \\ & & -\Psi & I \end{bmatrix} \approx \begin{bmatrix} I & & & \\ -\Phi^m & I & & \\ & \ddots & \ddots & \\ & & -\Phi^m & I \end{bmatrix} \quad (3)$$

is the coarse-grid operator with Ψ denoting the *coarse-grid time-stepping operator* that approximates Φ^m , and \mathbf{e}_Δ is an approximate error at C-points. In the two-grid setting analyzed in this paper, this reduced system is solved exactly via sequential time-stepping on the coarse grid, but in the multilevel setting it is solved approximately by recursively applying MGRIT, noting that A_1 has the same block bidiagonal structure as A_0 in (2). Upon computing the approximate error \mathbf{e}_Δ , it is added to C-point values of \mathbf{w} , and then the post-relaxation is performed.

When $\Psi = \Phi^m$, $A_1 e_\Delta = r_\Delta$ is exactly the C-point Schur complement of the residual equation $A_0 e = r$, in which $e = u - w$ is the algebraic error, and MGRIT converges exactly in a single iteration; thus, we dub Φ^m the *ideal coarse-grid time-stepping operator*. No parallel speed-up can be obtained by using $\Psi = \Phi^m$, however, since the sequential coarse-grid solve is as expensive as solving the original fine-grid problem. The convergence of MGRIT is naturally determined by the accuracy of the approximation $\Psi \approx \Phi^m$, where one needs to strike a balance between the complexity or the cost of applying Ψ , and the accuracy of the approximation of Φ^m . In the PDE context, the most common approach for computing Ψ is to rediscritize the fine-grid problem using the enlarged coarse-grid time step $m\delta t$, which tends to work well for diffusion-dominated problems. For advection-dominated problems, however, this typically leads to extremely poor convergence, for which we provide theoretical insight in Section 6, based on results derived in Sections 3 and 4.

2.2 | Assumptions and notation

The analysis in this paper relies on the following assumptions on the time-stepping operators.

Assumption 1 (Simultaneous diagonalizability). The fine- and coarse-grid time-stepping operators $\Phi \in \mathbb{R}^{n_x \times n_x}$ and $\Psi \in \mathbb{R}^{n_x \times n_x}$ are simultaneously diagonalizable by a unitary matrix U ,

$$\Phi = U \operatorname{diag}(\lambda_1, \dots, \lambda_{n_x}) U^*, \quad \Psi = U \operatorname{diag}(\mu_1, \dots, \mu_{n_x}) U^*, \quad (4)$$

with λ_i and μ_i denoting the i th eigenvalue of Φ and Ψ , respectively.

Simultaneous diagonalizability allows the convergence analysis of MGRIT to be simplified immensely, and it has appeared in previous analyses for this reason.^{8, 28, 29, 31, 32} We also place an assumption on the stability of Φ and Ψ , as follows.

Assumption 2 (Stability). The fine- and coarse-grid time-stepping operators are ℓ^2 -stable, with $\|\Phi\|_2, \|\Psi\|_2 < 1$. Or equivalently, $|\lambda_i|, |\mu_i| < 1, \forall i \in \{1, \dots, n_x\}$.

Remark 1. Unit eigenvalues. It is not difficult to show that if there is an eigenvector for which $\lambda_{i_*} = \mu_{i_*} = 1$, then MGRIT exactly eliminates error in this direction in a single iteration (see Appendix A, Lemma 4). Such unit eigenvalues often arise for PDEs with periodic spatial boundary conditions, where they are associated with the constant eigenvector, for example. So, the reader should assume that Assumption 2 holds in terms of our analysis, but note that having unit eigenvalues does not present additional difficulties.

For our analysis, it is also necessary to introduce the lower shift matrix L_n , and the Vandermonde-style function $v : \mathbb{C}^{n \times n} \rightarrow \mathbb{C}^{mn \times n}$ defined by

$$L_n := \begin{bmatrix} 0 & & & \\ 1 & 0 & & \\ & \ddots & \ddots & \\ & & 1 & 0 \end{bmatrix} \in \mathbb{R}^{n \times n}, \quad v(X) := \begin{bmatrix} I \\ X \\ \vdots \\ X^{m-1} \end{bmatrix}. \quad (5)$$

3 | ERROR PROPAGATION

Suppose $u^{(p)}$ is the approximation to the solution of $A_0 u = b$ after p MGRIT iterations, and that $e^{(p)} = u - u^{(p)}$ is the algebraic error in that approximation. Then, the error propagator \mathcal{E} transforms the initial error $e^{(0)}$ as $e^{(p)} = \mathcal{E}^p e^{(0)}$. Thus, the spectral properties of \mathcal{E}^p characterize the convergence of the iteration. For example, the norm and spectral radius of \mathcal{E} describe the short-term and asymptotic convergence behaviors of the method, respectively. The error propagator for a two-grid multigrid method takes the form (see Trottenberg et al.,³⁷ Section 2.2.3)

$$\mathcal{E} = S_{\text{post}} \mathcal{K} S_{\text{pre}}, \quad \text{where } \mathcal{K} = I - P A_1^{-1} R A_0, \quad (6)$$

where A_0, A_1 represent the fine- and coarse-grid matrices, and S_{pre} and S_{post} denote error propagators for pre- and post relaxation, respectively. The error propagator \mathcal{K} is that of the coarse-grid correction, in which R and P denote the restriction and interpolation operators, respectively. We note that there are several equivalent formulations of the MGRIT error propagator. We follow References 28, Section 4.1.3, & 29, by considering the propagator on the fine grid, although similar results can be obtained by considering only coarse-grid degrees-of-freedom, as in References 8, 28, 31, 32. Similarly, we take P in the above

to be injection interpolation, while other works use so-called ideal interpolation, in which the interpolation P also incorporates the post-relaxation from the MGRIT iteration.^{3, 13, 29–32}

As noted above, and as described in Section 2.1, in this work we fix the interpolation and restriction operators in (6) as injection, writing P for injection from the coarse-grid points into the fine grid, and P^\top for its adjoint. We also fix the post-relaxation to be S^F , with pre-relaxation as $(S^{CF})^\nu S^F$ for some $\nu \in \mathbb{N}_0$, yielding

$$\mathcal{E} = S^F \mathcal{K} (S^{CF})^\nu S^F, \quad \text{where } \mathcal{K} = I - P A_1^{-1} P^\top A_0. \quad (7)$$

Expressions for P , S^F , and S^{CF} , are derived, for example, in References 8, 28, 29, 31, 32, so we omit them here, but include their derivations in Appendix B.

3.1 | Temporal MGRIT error propagation

Since Φ and Ψ are simultaneously unitarily diagonalizable (see Assumption 1), their eigenvectors \mathcal{U} can be used to transform (7) into a block diagonal matrix. More specifically, one has

$$\mathcal{E} \xrightarrow{\text{unitary similarity transform}} \check{\mathcal{E}} = \text{diag} (\mathcal{E}_i) \in \mathbb{C}^{n_x n_t \times n_x n_t}, \quad 1 \leq i \leq n_x. \quad (8)$$

The unitary matrix involved in this transform can be written as the composition $(I_{n_t} \otimes \mathcal{U})\mathcal{P}$, in which \mathcal{P} is a permutation matrix reordering space-time vectors from the original ordering where all spatial degrees of freedom (DOFs) at a single time point are blocked together, to one in which all temporal DOFs belonging at a single spatial point are blocked together.^{8, 28, 29, 31, 32} Since a unitary similarity transform of a matrix preserves its ℓ^2 -norm and eigenvalues, (8) simplifies the task of computing the norm and spectral radius of $\mathcal{E} \in \mathbb{C}^{n_x n_t \times n_x n_t}$ into one of computing norms and spectral radii of n_x error propagators $\mathcal{E}_i \in \mathbb{C}^{n_t \times n_t}$. The i th diagonal block in (8) takes the form

$$\mathcal{E}_i = S_i^F \left(I_{n_t} - P_i A_{1,i}^{-1} P_i^\top A_{0,i} \right) (S_i^{CF})^\nu S_i^F \in \mathbb{C}^{n_t \times n_t}, \quad (9)$$

and it characterizes the evolution of an error vector in the direction of the i th eigenvector of Φ and Ψ . In other words, the effect of the similarity transform (8) has been to decouple the space-time equation $\mathbf{e}^{(1)} = \mathcal{E} \mathbf{e}^{(0)}$ into n_x time-only problems, with the i th such problem representing error propagation of the i th spatial eigenvector.

The constituent terms in (9) are found by applying the similarity transform from (8) to the components of \mathcal{E} in (7). These can be written as

$$A_{0,i} = I_{n_t} - \lambda_i L_{n_t} \in \mathbb{C}^{n_t \times n_t}, \quad (10)$$

$$A_{1,i} = I_{n_t/m} - \mu_i L_{n_t/m} \in \mathbb{C}^{n_t/m \times n_t/m}, \quad (11)$$

$$P_i = I_{n_t/m} \otimes \mathbf{e}_1 \in \mathbb{C}^{n_t \times n_t/m}, \quad (12)$$

$$S_i^F = I_{n_t/m} \otimes [\nu(\lambda_i) \mathbf{e}_1^\top] \in \mathbb{C}^{n_t \times n_t}, \quad (13)$$

$$S_i^{CF} = L_{n_t/m} \otimes [\lambda_i \nu(\lambda_i) \mathbf{e}_m^\top] \in \mathbb{C}^{n_t \times n_t}. \quad (14)$$

Here, $\mathbf{e}_1, \mathbf{e}_m \in \mathbb{R}^m$ are the canonical (column-oriented) basis vectors in the first and m th directions, respectively. Recall the matrix L_n and function ν are defined in (5).

4 | LOCAL FOURIER ANALYSIS

In this section, LFA is used to analyze the temporal MGRIT error propagators \mathcal{E}_i in (9). The framework for the analysis is described in Section 4.1, key intermediate computations for the theory are given in Section 4.2, and the main theoretical results are given in Section 4.3. Note that the convergence theory developed in this section applies to general Φ and Ψ satisfying the assumptions described earlier, and specific implications of this theory for advection-dominated PDEs will be described in Section 6.

4.1 | Introduction and preliminaries

To analyze the two-grid problem with LFA, we consider it posed on a pair of semi-infinite temporal grids, and we ignore the influence and effects of boundary conditions by replacing the initial condition at $t = 0$ and the outflow condition at the final time with a periodic boundary condition. To this end, with ℓ denoting the level in the multigrid hierarchy, we associate the semi-infinite temporal grids

$$\mathbf{G}_\ell := \{t_k = km^\ell \delta t : k \in \mathbb{N}_0\}, \quad \ell \in \{0, 1\}. \quad (15)$$

On the grids \mathbf{G}_ℓ , we consider the infinite-dimensional extension of matrix \mathcal{E}_i in (9) and of the matrices in (10)–(14) that compose it. In addition, we consider the following Fourier modes on grids (15) with continuously varying frequency θ :

$$\varphi_\ell(\theta, t) := \exp\left(\frac{i\theta t}{m^\ell \delta t}\right), \quad t \in \mathbf{G}_\ell, \quad \theta \in \Theta_\ell, \quad (16)$$

with

$$\Theta_\ell = \begin{cases} \left[-\frac{\pi}{m}, 2\pi - \frac{\pi}{m}\right), & \ell = 0, \\ [-\pi, \pi) & \ell = 1. \end{cases} \quad (17)$$

Any intervals of length 2π could be used for Θ_ℓ , but these choices provide some notational simplifications.²⁸ We adopt the shorthand $\boldsymbol{\varphi}_\ell(\theta)$ for denoting the vector that is populated with the Fourier mode (16) sampled at all time points $t \in \mathbf{G}_\ell$. The modes $\boldsymbol{\varphi}_\ell(\theta)$ lie at the heart of LFA because they are formally eigenfunctions of any infinite-dimensional Toeplitz operator that acts on the grid \mathbf{G}_ℓ .^{37, 38}

On \mathbf{G}_ℓ , we introduce the scaled Hermitian inner product of two grid functions $a_\ell, b_\ell : \mathbf{G}_\ell \rightarrow \mathbb{C}$ as

$$\langle a_\ell, b_\ell \rangle := \lim_{n_t \rightarrow \infty} \frac{1}{n_t} \sum_{k=0}^{n_t-1} \bar{a}_\ell(t_k) b_\ell(t_k), \quad (18)$$

where $\bar{a}(t_k)$ denotes the complex conjugate of $a(t_k)$. Note that the Fourier modes (16) are orthonormal with respect to this inner product.

We partition the frequency space Θ_0 into two disjoint sets according to

$$\Theta^{\text{low}} := \left[-\frac{\pi}{m}, \frac{\pi}{m}\right), \quad \Theta^{\text{high}} := \left[\frac{\pi}{m}, 2\pi - \frac{\pi}{m}\right). \quad (19)$$

Observe that for any $\theta \in \Theta^{\text{low}}$, we have $\varphi_0\left(\theta + \frac{2\pi\alpha}{m}, t\right) = \frac{1}{\sqrt{m}} \varphi_1(m\theta, t)$ for all $t \in \mathbf{G}_1$ and $\alpha \in \{0, \dots, m-1\}$. These m fine-grid functions, $\varphi_0\left(\theta + \frac{2\pi\alpha}{m}, t\right)$, are known as *harmonics* of one another. The fact that the harmonics are indistinguishable from one another when sampled on the coarse-grid points is the motivation for the partitioning in (19) (see De Sterck et al.,²⁸ Section 4.1.2). A second useful fact is that constant-stencil interpolation and restriction operators map the function $\varphi_1(m\theta, t)$ for $\theta \in \Theta^{\text{low}}$ onto the associated harmonic functions and vice-versa, leading to the definition of the m -dimensional spaces of harmonics.

Definition 1 ($m\delta t$ -harmonics). For a given $\theta \in \Theta^{\text{low}}$, the associated m -dimensional space of harmonics is

$$\mathcal{H}_{\delta t}^\theta := \text{span}_{0 \leq \alpha < m} \left\{ \varphi_0\left(\theta + \frac{2\pi\alpha}{m}\right) \right\}. \quad (20)$$

As we will show, $\mathcal{H}_{\delta t}^\theta$ is also an invariant subspace of both C- and F-relaxation, although each Fourier mode is not an eigenfunction. Thus, for a given $\theta \in \Theta^{\text{low}}$, the action of the various MGRIT components (10)–(14) on Fourier modes (16) is characterized by

$$A_{0,i} : \mathcal{H}_{\delta t}^\theta \rightarrow \mathcal{H}_{\delta t}^\theta, \quad (21)$$

$$A_{1,i} : \text{span}\{\varphi_1(m\theta)\} \rightarrow \text{span}\{\varphi_1(m\theta)\}, \quad (22)$$

$$P_i : \text{span}\{\varphi_1(m\theta)\} \rightarrow \mathcal{H}_{\delta t}^\theta, \quad (23)$$

$$S_i^F : \mathcal{H}_{\delta t}^\theta \rightarrow \mathcal{H}_{\delta t}^\theta, \quad (24)$$

$$S_i^{\text{CF}} : \mathcal{H}_{\delta t}^\theta \rightarrow \mathcal{H}_{\delta t}^\theta. \quad (25)$$

Note that the spans in (22) and (23) are over a one-dimensional set. Since the MGRIT error propagator \mathcal{E}_i is composed of the above operators (see (9)), it is invariant on the space of $m\delta t$ -harmonics:

$$\mathcal{E}_i : \mathcal{H}_{\delta t}^\theta \rightarrow \mathcal{H}_{\delta t}^\theta \quad \text{for all } \theta \in \Theta^{\text{low}}. \quad (26)$$

Therefore, by grouping together harmonic Fourier modes, the infinite-dimensional error propagator \mathcal{E}_i can be block diagonalized. Specifically, the transformed operator has one diagonal block $\hat{\mathcal{E}}_i(\theta) \in \mathbb{C}^{m \times m}$ associated with each $\theta \in \Theta^{\text{low}}$, where, for a given $\theta \in \Theta^{\text{low}}$, $\hat{\mathcal{E}}_i(\theta)$ is the representation of \mathcal{E}_i on the harmonic space $\mathcal{H}_{\delta t}^\theta$. That is,

$$\mathcal{E}_i \xrightarrow{\text{unitary similarity transform}} \text{diag}_{\theta \in \Theta^{\text{low}}} (\hat{\mathcal{E}}_i(\theta)). \quad (27)$$

We call $\hat{\mathcal{E}}_i(\theta)$ the *Fourier symbol* of \mathcal{E}_i associated with the harmonic space $\mathcal{H}_{\delta t}^\theta$ (or just the Fourier symbol of \mathcal{E}_i for short).

Let $V(\theta)$ be a matrix with m columns given by the m harmonic Fourier modes from (20):

$$V(\theta) := \begin{bmatrix} \varphi_0(\theta) & \varphi_0\left(\theta + \frac{2\pi}{m}\right) & \dots & \varphi_0\left(\theta + \frac{2\pi(m-1)}{m}\right) \end{bmatrix}. \quad (28)$$

Then, the Fourier symbol arising in the similarity transform (27) associated with $\mathcal{H}_{\delta t}^\theta$ satisfies $\mathcal{E}_i V(\theta) = V(\theta) \hat{\mathcal{E}}_i(\theta)$. Since V has orthonormal columns, the Fourier symbol itself can be written $\hat{\mathcal{E}}_i(\theta) = V^*(\theta) \mathcal{E}_i V(\theta) \in \mathbb{C}^{m \times m}$. Since the ℓ^2 -norm and the eigenvalues of a matrix are preserved under a unitary similarity transform, from (27) we have

$$\|\mathcal{E}_i\|_2 = \sup_{\theta \in \Theta^{\text{low}}} \|\hat{\mathcal{E}}_i(\theta)\|_2, \quad \rho(\mathcal{E}_i) = \sup_{\theta \in \Theta^{\text{low}}} \rho(\hat{\mathcal{E}}_i(\theta)). \quad (29)$$

Thus, the computation of the norm and spectral radius of the infinite-dimensional \mathcal{E}_i has been reduced to the computation of these quantities on an infinite number of finite-dimensional matrices, $\hat{\mathcal{E}}_i(\theta) \in \mathbb{C}^{m \times m}$, $\theta \in \Theta^{\text{low}}$.

From the definition of \mathcal{E}_i in (9), the error propagator $\hat{\mathcal{E}}_i(\theta)$ takes the form

$$\hat{\mathcal{E}}_i(\theta) = \hat{S}_i^F(\theta) \hat{\mathcal{K}}_i(\theta) (\hat{S}_i^{\text{CF}}(\theta))^* \hat{S}_i^F(\theta) \in \mathbb{C}^{m \times m}, \quad (30)$$

where $\hat{\mathcal{K}}_i(\theta)$ is the Fourier symbol of the coarse-grid correction,

$$\hat{\mathcal{K}}_i(\theta) = I_m - \hat{P}_i(\theta) [\hat{A}_{1,i}(m\theta)]^{-1} \hat{P}_i^T(\theta) \hat{A}_{0,i}(\theta) \in \mathbb{C}^{m \times m}. \quad (31)$$

The component matrices used in (30) and (31) are the Fourier symbols of the infinite-dimensional extensions of the multigrid components defined in (10)–(14). From (21)–(25), these Fourier symbols may be expressed as

$$\hat{A}_{0,i}(\theta) = V^*(\theta) A_{0,i} V(\theta) \in \mathbb{C}^{m \times m}, \quad (32)$$

$$\hat{A}_{1,i}(m\theta) = \varphi_1^*(m\theta) A_{1,i} \varphi_1(m\theta) \in \mathbb{C}, \quad (33)$$

$$\hat{P}_i(\theta) = V^*(\theta) P_i \varphi_1(m\theta) \in \mathbb{C}^m, \quad (34)$$

$$\hat{S}_i^F(\theta) = V^*(\theta) S_i^F V(\theta) \in \mathbb{C}^{m \times m}, \quad (35)$$

$$\hat{S}_i^{\text{CF}}(\theta) = V^*(\theta) S_i^{\text{CF}} V(\theta) \in \mathbb{C}^{m \times m}. \quad (36)$$

4.2 | Derivations of Fourier symbols

Deriving expressions for the Fourier symbols (30)–(36) is a straightforward, but tedious calculation. Here, we state the main results, but defer their proofs to Appendix C. We note that the LFA theory in De Sterck et al.²⁸ also derived Fourier symbols for MGRIT; however, De Sterck et al.²⁸ used both a different basis than that in (28) and an alternative formulation of the error-propagation operator, so the expressions derived here do not match those there. Furthermore, the analysis in De Sterck et al.²⁸ focused on numerical evaluation of the LFA convergence estimates, while the focus here will be to algebraically manipulate the Fourier symbols in order to give closed-form convergence estimates.

4.2.1 | Fourier symbols of fine- and coarse-grid operators, and interpolation

Since $A_{0,i}$ in (10) and $A_{1,i}$ in (11) are infinite-dimensional Toeplitz operators, the Fourier modes $\varphi_\ell(\theta)$ are their eigenfunctions and, so, their Fourier symbols are simply

$$\hat{A}_{i,0}(\theta) = \text{diag}_{0 \leq \alpha < m} \left(\tilde{A}_{0,i} \left(\theta + \frac{2\pi\alpha}{m} \right) \right) \in \mathbb{C}^{m \times m}, \quad \hat{A}_{1,i}(m\theta) = \tilde{A}_{1,i}(m\theta) \in \mathbb{C}. \quad (37)$$

Here, $\tilde{A}_{\ell,i}(\theta)$ is the eigenvalue or Fourier symbol of A_i associated with the eigenfunction $\boldsymbol{\varphi}_\ell(\theta)$. Due to the lower bidiagonal structure of A_i , these Fourier symbols are given by

$$\tilde{A}_{0,i}(\theta) = 1 - \lambda_i e^{-i\theta} \in \mathbb{C}, \quad \tilde{A}_{1,i}(m\theta) = 1 - \mu_i e^{-im\theta} \in \mathbb{C}. \quad (38)$$

We next consider the Fourier symbol of interpolation (34), which can be derived by considering its transpose, which is restriction by injection. Recall that for any $\theta \in \Theta^{\text{low}}$, $\varphi_0\left(\theta + \frac{2\pi\alpha}{m}, t\right) = \frac{1}{\sqrt{m}}\varphi_1(m\theta, t)$ for time points $t \in \mathbf{G}_1$, where $\alpha \in \{0, \dots, m-1\}$. Thus, injection of the values of $\varphi_0\left(\theta + \frac{2\pi\alpha}{m}, t\right)$ at time points $t \in \mathbf{G}_1$ maps any fine-grid harmonic to the associated coarse-grid Fourier mode $\varphi_1(m\theta, t)$, with its amplitude scaled by $\frac{1}{\sqrt{m}}$. Thus, the Fourier symbol of injection restriction is $\frac{1}{\sqrt{m}}\mathbf{1}^\top$, where $\mathbf{1} \in \mathbb{R}^m$ denotes a column vector of ones. Note that when interpolation is the adjoint of restriction, its Fourier symbol is the adjoint of that of restriction up to some constant scaling (see, e.g., Remark 4.4.3 in Trottenberg et al.³⁷), with injection representing the case in which the scaling is unity. Therefore the Fourier symbol of injection interpolation is simply

$$\hat{P}_i(\theta) = \frac{1}{\sqrt{m}}\mathbf{1}. \quad (39)$$

4.2.2 | Relaxation Fourier symbols

We now compute the relaxation Fourier symbols (35) and (36). These Fourier symbols are more complicated than those in the previous section because they intermix harmonics in a non-trivial way.

Lemma 1 (F-relaxation Fourier symbol). The Fourier symbol (35) of F-relaxation may be written as the following rank-1 matrix

$$\hat{S}_i^F(\theta) = c(\theta) [\hat{A}_{0,i}(\theta)]^{-1} \mathbf{1} \mathbf{1}^\top, \quad (40)$$

in which $\hat{A}_{0,i}(\theta)$ is given in (37), and $c(\theta)$ is the function

$$c(\theta) := \frac{1}{m} [1 - (\lambda_i e^{-i\theta})^m]. \quad (41)$$

Proof. See Appendix C.1. □

The fact that $\hat{S}_i^F(\theta)$ is dense reflects that F-relaxation couples together the m harmonics in $\mathcal{H}_{\delta t}^\theta$ (see Definition 1). This contrasts with simple relaxation methods typically used in the multigrid solution of Poisson problems, for example, for which the Fourier symbol of relaxation is diagonal (or block diagonal), representing that harmonics are not mixed (or partially mixed) by relaxation.³⁷

Recall that F-relaxation updates F-point values to have zero residuals while leaving C-point values unchanged. Thus, after an initial F-relaxation successive F-relaxations have no effect since F-point residuals are already zero. The following useful result shows that the Fourier symbol $\hat{S}_i^F(\theta)$ for F-relaxation inherits this property.

Corollary 1 (Idempotence of F-relaxation). The Fourier symbol $\hat{S}_i^F(\theta)$ for F-relaxation, as given by (40), is idempotent: $\hat{S}_i^F(\theta) \hat{S}_i^F(\theta) = \hat{S}_i^F(\theta)$. Furthermore, $\hat{S}_i^F(\theta)$ has a single eigenvalue of unity, and $m-1$ eigenvalues that are zero.

Proof. See Appendix C.2. □

Having identified the Fourier symbol for F-relaxation in Lemma 1, we now consider the Fourier symbol for CF-relaxation and that of pre-relaxation as a whole.

Lemma 2 (Pre-relaxation Fourier symbol). The Fourier symbol (36) for CF-relaxation may be expressed as

$$\hat{S}_i^{\text{CF}}(\theta) = \hat{S}_i^F(\theta) [I - \hat{A}_{0,i}(\theta)], \quad (42)$$

where $\hat{S}_i^F(\theta)$ is given by (40), and $\hat{A}_{0,i}(\theta)$ is given in (37). Furthermore, the Fourier symbol for the entire pre-relaxation operator in (30) may be expressed as

$$(\hat{S}_i^{\text{CF}}(\theta))^\nu \hat{S}_i^F(\theta) = (\lambda_i e^{-i\theta})^{m\nu} \hat{S}_i^F(\theta), \quad \nu \in \mathbb{N}_0. \quad (43)$$

Proof. See Appendix C.3. □

4.2.3 | Error propagator Fourier symbol

Having computed convenient representations for the Fourier symbols that compose the Fourier symbol for the error propagator in (30), we now compute this Fourier symbol itself.

Theorem 1 (Error propagator Fourier symbol). The error propagator Fourier symbol (30) may be written as

$$\hat{\mathcal{E}}_i(\theta) = f(\theta)\hat{S}_i^F(\theta), \quad (44)$$

where $\hat{S}_i^F(\theta)$ is the Fourier symbol for F-relaxation given in (40), and $f(\theta)$ is

$$f(\theta) := (\lambda_i e^{-i\theta})^{mv} \frac{\lambda_i^m - \mu_i}{e^{im\theta} - \mu_i}. \quad (45)$$

Proof. See Appendix C.4. □

4.3 | LFA convergence estimates

In this section, we present our main theoretical results on the LFA estimates for error propagation, which are based on the *simple* representation of the error propagator Fourier symbol given in Theorem 1. We begin with the norm of this matrix.

Theorem 2 (Error propagator Fourier symbol norm). The ℓ^2 -norm of the Fourier symbol for the error propagator given in Theorem 1 is

$$\|\hat{\mathcal{E}}_i(\theta)\|_2 = |\lambda_i|^{mv} \frac{|\lambda_i^m - \mu_i|}{|e^{im\theta} - \mu_i|} \sqrt{\frac{1 - |\lambda_i|^{2m}}{1 - |\lambda_i|^2}}. \quad (46)$$

Proof. Using (44), the squared norm of $\hat{\mathcal{E}}_i(\theta)$ can be expressed as

$$\|\hat{\mathcal{E}}_i(\theta)\|_2^2 = \rho(\hat{\mathcal{E}}_i^*(\theta)\hat{\mathcal{E}}_i(\theta)) = |f(\theta)|^2 \rho((\hat{S}_i^F(\theta))^* \hat{S}_i^F(\theta)). \quad (47)$$

Substituting $\hat{S}_i^F(\theta) = c(\theta)[\hat{A}_{0,i}(\theta)]^{-1}\mathbf{1}\mathbf{1}^\top$ from (40), this becomes

$$\|\hat{\mathcal{E}}_i(\theta)\|_2^2 = |f(\theta)|^2 \rho\left(\left[\mathbf{1}\mathbf{1}^\top \bar{c}(\theta)[\hat{A}_{0,i}^*(\theta)]^{-1}\right] \left[c(\theta)[\hat{A}_{0,i}(\theta)]^{-1}\mathbf{1}\mathbf{1}^\top\right]\right), \quad (48)$$

$$= |f(\theta)|^2 \rho\left(\left[\mathbf{1}^\top \bar{c}(\theta)[\hat{A}_{0,i}^*(\theta)]^{-1}c(\theta)[\hat{A}_{0,i}(\theta)]^{-1}\mathbf{1}\right]\mathbf{1}\mathbf{1}^\top\right), \quad (49)$$

$$= m|f(\theta)|^2 \left(\mathbf{1}^\top \bar{c}(\theta)[\hat{A}_{0,i}^*(\theta)]^{-1}c(\theta)[\hat{A}_{0,i}(\theta)]^{-1}\mathbf{1}\right). \quad (50)$$

To arrive at (50), note that the term in the closed parenthesis multiplying $\mathbf{1}\mathbf{1}^\top$ in (49) is a non-negative scalar, and that $\rho(\mathbf{1}\mathbf{1}^\top) = \mathbf{1}^\top \mathbf{1} = m$.

Now we consider the inner product in (50). Using the identity of (C28) for the p th element, $p \in \{0, \dots, m-1\}$, of $c(\theta)[\hat{A}_{0,i}(\theta)]^{-1}\mathbf{1}$, we have

$$\left[c(\theta)[\hat{A}_{0,i}(\theta)]^{-1}\mathbf{1}\right]_p = \frac{1}{m} \sum_{r=0}^{m-1} [\lambda_i \exp(-i(\theta + \frac{2\pi p}{m}))]^r. \quad (51)$$

Using (51), the inner product of concern can thus be written as

$$\begin{aligned} \mathbf{1}^\top \bar{c}(\theta)[\hat{A}_{0,i}^*(\theta)]^{-1}c(\theta)[\hat{A}_{0,i}(\theta)]^{-1}\mathbf{1} &= \sum_{p=0}^{m-1} \left(\left[\mathbf{1}^\top \bar{c}(\theta)[\hat{A}_{0,i}^*(\theta)]^{-1}\right]_p \left[c(\theta)[\hat{A}_{0,i}(\theta)]^{-1}\mathbf{1}\right]_p \right), \\ &= \frac{1}{m^2} \sum_{p=0}^{m-1} \left(\sum_{r=0}^{m-1} [\lambda_i \exp(-i(\theta + \frac{2\pi p}{m}))]^r \sum_{s=0}^{m-1} [\bar{\lambda}_i \exp(i(\theta + \frac{2\pi p}{m}))]^s \right), \end{aligned} \quad (52)$$

$$= \frac{1}{m^2} \sum_{p=0}^{m-1} \sum_{r=0}^{m-1} \sum_{s=0}^{m-1} \lambda_i^r \bar{\lambda}_i^s e^{i\theta(s-r)} \exp\left(\frac{2\pi i p(s-r)}{m}\right), \quad (53)$$

$$= \frac{1}{m^2} \sum_{r=0}^{m-1} \sum_{s=0}^{m-1} \lambda_i^r \bar{\lambda}_i^s e^{i\theta(s-r)} \left(\sum_{p=0}^{m-1} \exp\left(\frac{2\pi i p(s-r)}{m}\right) \right). \quad (54)$$

Slightly rewriting it, the geometric sum in parentheses in (54) is

$$\sum_{p=0}^{m-1} \left[\exp \left(\frac{2\pi i(s-r)}{m} \right) \right]^p = \begin{cases} m, & \text{if } (s-r) \bmod m = 0, \\ 0, & \text{else.} \end{cases} \quad (55)$$

In (54), $r, s \in \{0, \dots, m-1\}$, and, thus, $s-r \in \{1-m, \dots, m-1\}$. Therefore, the only time that $s-r$ is an integer multiple of m is when $s-r=0$, or $r=s$. As such, (55) is equal to $m\delta_{r,s}$, where δ is the Kronecker delta function. Substituting this result into (54) gives

$$\mathbf{1}^\top \bar{c}(\theta) [\hat{A}_{0,i}^*(\theta)]^{-1} c(\theta) [\hat{A}_{0,i}(\theta)]^{-1} \mathbf{1} = \frac{1}{m^2} \sum_{r=0}^{m-1} \sum_{s=0}^{m-1} \lambda_i^r \bar{\lambda}_i^s e^{i\theta(s-r)} m\delta_{r,s} = \frac{1}{m} \sum_{r=0}^{m-1} \lambda_i^r \bar{\lambda}_i^r = \frac{1}{m} \frac{1 - |\lambda_i|^{2m}}{1 - |\lambda_i|^2}, \quad (56)$$

with the final equality following from the prior expression being a geometric sum in $|\lambda_i|^2$.

The claimed result (46) follows by substituting (56) into (50) along with the value of $|f(\theta)|^2$ coming from (45), and then taking the square root of the result. \square

Recall from (29) that the norm of \mathcal{E}_i is given by the maximum norm of its Fourier symbols $\hat{\mathcal{E}}_i(\theta)$ over $\theta \in \Theta^{\text{low}}$.

Theorem 3 (Error propagator norm). The ℓ^2 -norm of the error propagator \mathcal{E}_i defined in (9) is

$$\|\mathcal{E}_i\|_2 = \sup_{\theta \in \Theta^{\text{low}}} \|\hat{\mathcal{E}}_i(\theta)\|_2 = |\lambda_i|^{mv} \frac{|\lambda_i^m - \mu_i|}{1 - |\mu_i|} \sqrt{\frac{1 - |\lambda_i|^{2m}}{1 - |\lambda_i|^2}}. \quad (57)$$

Furthermore, of all harmonic spaces $\mathcal{H}_{\delta t}^\theta$ with $\theta \in \Theta^{\text{low}}$ from Definition 1, the one with the least error reduction is that associated with frequency $\theta = \theta_i^\dagger$, where

$$\theta_i^\dagger := \arg \max_{\theta \in \Theta^{\text{low}}} \|\hat{\mathcal{E}}_i(\theta)\|_2 = \frac{1}{m} \arg \mu_i, \quad (58)$$

in which $\arg \mu_i$ denotes the argument of the complex number μ_i .

Proof. The first equality in (57) was already given as (29). Let us first consider the slowest converging harmonic space, and then return to the second equality in (57). From the expression for $\|\hat{\mathcal{E}}_i(\theta)\|_2$ given in (46), the only dependence on frequency θ is via the term $\frac{1}{|e^{im\theta} - \mu_i|}$. Therefore, we have

$$\theta_i^\dagger := \arg \max_{\theta \in \Theta^{\text{low}}} \|\hat{\mathcal{E}}_i(\theta)\|_2 = \arg \max_{\theta \in \Theta^{\text{low}}} \frac{1}{|e^{im\theta} - \mu_i|} = \arg \min_{\theta \in \Theta^{\text{low}}} |e^{im\theta} - \mu_i|. \quad (59)$$

Furthermore, since Θ^{low} is the continuous frequency space spanning $[-\frac{\pi}{m}, \frac{\pi}{m}]$ (see (19)), introducing the new variable $\vartheta = m\theta$ gives

$$\min_{\theta \in \Theta^{\text{low}}} |e^{im\theta} - \mu_i| = \min_{\vartheta \in [-\pi, \pi]} |e^{i\vartheta} - \mu_i|. \quad (60)$$

This is simply the shortest distance from the unit circle to the complex number μ_i that lies inside it (recall that $|\mu_i| < 1$ under Assumption 2). By a simple geometric argument, this distance is minimized by the point on the unit circle having the same argument as μ_i ; that is, the minimum over $\vartheta \in [-\pi, \pi]$ is achieved at $\vartheta = \arg \mu_i$. Since $\theta = \vartheta/m$, the minimizing frequency over $\theta \in \Theta^{\text{low}}$ is simply $\theta_i^\dagger = \frac{1}{m} \arg \mu_i$.

To evaluate this minimum distance, write μ_i in polar form as $\mu_i = |\mu_i| e^{i \arg \mu_i}$ and substitute it into the above equation to yield

$$\min_{\theta \in \Theta^{\text{low}}} |e^{im\theta} - \mu_i| = |e^{i \arg \mu_i} - |\mu_i| e^{i \arg \mu_i}| = |1 - |\mu_i|| e^{i \arg \mu_i}| = 1 - |\mu_i|, \quad (61)$$

with the last equality following since $|\mu_i| < 1$. Finally, the result (57) follows by evaluating $\|\hat{\mathcal{E}}_i(\theta_i^\dagger)\|_2$ from (46) using the fact that $|e^{im\theta_i^\dagger} - \mu_i| = 1 - |\mu_i|$. \square

Given the structure of the Fourier symbol $\hat{\mathcal{E}}_i(\theta)$ in Theorem 1, and the result from Theorem 3, it is straightforward to compute the spectral radius of \mathcal{E}_i .

Corollary 2 (Error propagator spectral radius). The spectral radius of the error propagator Fourier symbol $\hat{\mathcal{E}}_i(\theta)$ given in Theorem 1 is

$$\rho(\hat{\mathcal{E}}_i(\theta)) = |\lambda_i|^{mv} \frac{|\lambda_i^m - \mu_i|}{|e^{im\theta} - \mu_i|}. \quad (62)$$

Furthermore, the spectral radius of the error propagator \mathcal{E}_i given in (9) is

$$\rho(\mathcal{E}_i) = \sup_{\theta \in \Theta^{\text{low}}} \rho(\hat{\mathcal{E}}_i(\theta)) = \rho(\hat{\mathcal{E}}_i(\theta_i^\dagger)) = |\lambda_i|^{mv} \frac{|\lambda_i^m - \mu_i|}{1 - |\mu_i|}. \quad (63)$$

Proof. From the expression for $\hat{\mathcal{E}}_i(\theta)$ given in (44), its spectral radius is simply

$$\rho(\hat{\mathcal{E}}_i(\theta)) = \rho(f(\theta)\hat{S}_i^F(\theta)) = |f(\theta)|\rho(\hat{S}_i^F(\theta)) = |f(\theta)|, \quad (64)$$

with the final equality following as an immediate consequence of Corollary 1. Substituting $f(\theta)$ from its definition given in (45) gives the claimed result of (62).

The first equality in (63) was already given as (29). The second equality follows from θ_i^\dagger being the maximizer of $|e^{im\theta} - \mu_i|$, as shown in the proof of Theorem 3. \square

Remark 2. Rigorous Fourier analysis for time-periodic problems. While we have derived an LFA theory for the initial-value problem, our theory can be applied exactly or rigorously to a time-periodic MGRIT solver that employs a time-periodic coarse-grid equation (see, e.g., the solvers in References 41, 53). The reason for this is because the operators appearing in the time-periodic analogue of the error propagator (9) are (block) circulant. Therefore, the periodic Fourier modes $\phi_\ell(\theta)$ —with θ discretely sampled at n_t equidistant frequencies—are eigenfunctions for any finite n_t , and not only formally in the limit as $n_t \rightarrow \infty$ (as for the initial-value problem). See Section 3.4.4 of Trottenberg et al.³⁷ for a discussion on the link between rigorous and local Fourier analysis. Also note that our LFA theory bears a resemblance to the Fourier theory from Gander et al.⁴¹ for a time-periodic Parareal algorithm employing a time-periodic coarse-grid correction.

5 | COMPARISON TO EXISTING LITERATURE

The LFA results (57) and (63) from Section 4 bear a close resemblance to MGRIT convergence results in References 8, 28, 31, 32 obtained by other means. One salient difference is that References 8, 31, 32 analyze error propagation only over the coarse grid, following the argument that the use of ideal interpolation (or injection followed by F-relaxation) results in error dominated by its coarse-grid representation (see also Section 3). Further, References 8, 31, 32 consider the case of a finite temporal grid (finite n_t) and an initial-value problem. Our results apply rigorously (i.e., exactly) to time-periodic problems for finite n_t . Our results show also that LFA convergence estimates for the initial-value problem are similar to existing convergence bounds for the initial-value problem obtained by other means. In addition, as described earlier, our results extend the LFA theory from De Sterck et al.²⁸ in which Fourier symbols were derived, but they were not used in such a way as to derive analytical convergence estimates like those in Section 4.

This close resemblance to References 8, 28, 31, 32 described above is perhaps best seen by considering Southworth et al.⁴⁴—a companion article to Reference 32—because it gives results for fine-grid error propagation. Specifically, adopting our notation, and imposing Assumption 1, Corollary 3 of Southworth et al.⁴⁴ states that with FCF-relaxation (i.e., $\nu = 1$) the ℓ^2 -norm of the MGRIT error propagator (7) for finite n_t is

$$\|\mathcal{E}\|_2 = \max_{1 \leq i \leq n_x} |\lambda_i|^m \frac{|\lambda_i^m - \mu_i|}{1 - |\mu_i| + \mathcal{O}(1/N_c)} \sqrt{\frac{1 - |\lambda_i|^{2m}}{1 - |\lambda_i|^2}}. \quad (65)$$

Note that the formulation of \mathcal{E} used by Southworth et al.⁴⁴ is different than ours given by (7); however, they both represent the error propagator of the MGRIT algorithm and are, therefore, equivalent (accounting for different conventions for the sizes of the fine and coarse grids). In (65), N_c is the number of time points on the coarse grid, which is slightly different from the quantity of n_t/m that we have used. It is important to stress that (65) represents a genuine equality for finite n_t , up to the $\mathcal{O}(1/N_c)$ terms, unlike the LFA approximations considered in Section 4 which hold for the initial-value problem in the limit of infinite n_t .

Recalling our LFA approximation of $\|\mathcal{E}_i\|_2$ given by (57), and its relation to $\|\mathcal{E}\|_2$ given in (8), with FCF-relaxation our LFA theory gives the following *approximation* for finite n_t (for clarity, we write the LFA result following from (57) with $\nu = 1$

explicitly as an approximation here),

$$\|\mathcal{E}\|_2 = \max_{1 \leq i \leq n_x} \|\mathcal{E}_i\|_2 \approx \max_{1 \leq i \leq n_x} \sup_{\theta \in \Theta^{\text{low}}} \|\hat{\mathcal{E}}_i(\theta)\|_2 = \max_{1 \leq i \leq n_x} |\lambda_i|^m \frac{|\lambda_i^m - \mu_i|}{1 - |\mu_i|} \sqrt{\frac{1 - |\lambda_i|^{2m}}{1 - |\lambda_i|^2}}. \quad (66)$$

Comparing (66) and (65), they differ only by the small perturbation of $\mathcal{O}(1/N_c)$ appearing in (65). Moreover, as $n_t \rightarrow \infty$, and thus $N_c = \mathcal{O}(n_t/m) \rightarrow \infty$, the two expressions are equivalent. In other words, since (65) is valid for any value of n_t , it is consistent with our LFA approximation (66) holding exactly for $\|\mathcal{E}\|_2$ as $n_t \rightarrow \infty$. This consistency provides independent verification that our LFA theory of Section 4 is correct.

A key distinction of our theory compared to the those mentioned above is that it can naturally connect convergence issues for MGRIT to those of spatial multigrid methods for steady-state advection-dominated problems. Specifically, our theory can be used to describe convergence of space-time Fourier modes, while the above theories can only be used to describe convergence of spatial Fourier modes. It is precisely this retention of temporal Fourier information that makes our theory directly comparable with fully Fourier-based convergence theories in the steady-state spatial multigrid case. This comparison is studied in Section 6.

It is also interesting to note that our LFA approximation for the spectral radius of the error propagator (63) is the same as the bounds in Dobrev et al.⁸ Theorem 3.3 for the ℓ^2 -norm of the coarse-grid error propagator, provided one takes $n_t \rightarrow \infty$. In practice, MGRIT possesses a well-known exactness property that, in exactly $k = \frac{1}{v+1} \frac{n_t}{m}$ iterations, MGRIT converges to the exact solution of the fine-grid problem computed by sequentially time-stepping the initial condition across the time domain. As such, the spectral radius of the MGRIT error propagator is zero (for example, by Gelfand's formula) and does not provide useful information about pre-asymptotic convergence of the algorithm. Nonetheless, in References 8, 50, 51, (63) was shown to be an accurate prediction to the convergence factor measured in practice before the exactness property of MGRIT becomes dominant. Our LFA estimate of the spectral radius (which assumes periodicity-in-time and, thus, applies rigorously to cases outside of this exactness property) can, thus, be a reasonable predictor of the MGRIT convergence factor for these “middle iterations” of a time-parallel solve, which often determine the overall efficiency of the MGRIT methodology.

6 | CHARACTERISTIC COMPONENTS

We now use the LFA theory of Section 4 to shed light on the poor convergence of MGRIT for advection-dominated problems. General theoretical arguments and connections to spatial multigrid methods are presented in Section 6.1. Building on this, Section 6.2 theoretically analyzes MGRIT convergence for a class of semi-Lagrangian discretizations. Supporting numerical results are given in Section 6.3, and a discussion on the implications of these results as well as potential remedies for the slow convergence are given in Section 6.4.

This section makes use of a number of theoretical results that are rather lengthy to derive. In order not to distract from the key messages and findings of this section, many of these theoretical results and their proofs have been placed in Appendices D and E rather than in the main text.

6.1 | General theoretical arguments and connection to spatial multigrid methods

We now consider the constant-coefficient, one-dimensional advection-diffusion problem

$$\mathcal{A}u := \frac{\partial u}{\partial t} + \alpha \frac{\partial u}{\partial x} - \beta \frac{\partial^2 u}{\partial x^2} = 0, \quad (x, t) \in (-1, 1) \times (0, T], \quad u(x, 0) = u_0(x), \quad (67)$$

with $\alpha > 0$, $\beta \geq 0$, and $u(x, t)$ subject to periodic boundary conditions in space. Specifically, we analyze MGRIT convergence for discretizations of this problem by employing rigorous Fourier analysis in space and the LFA theory from Section 4. To this end, suppose that the space-time discretizations A_0 and A_1 given in (2) and (3), respectively, correspond to discretizations of \mathcal{A} on space-time meshes using n_x points in the x -direction separated by a distance of h .

Next, consider the space-time discretizations A_0 and A_1 on the semi-infinite space-time meshes \mathbf{M}_0 and \mathbf{M}_1 , respectively, which are defined by

$$\mathbf{M}_\ell := \left\{ (x, t) = (jh, km^\ell \delta t) : j \in \left\{ -\frac{n_x}{2}, \dots, \frac{n_x}{2} - 1 \right\}, k \in \mathbb{N}_0 \right\}, \quad \ell \in \{0, 1\}. \quad (68)$$

On \mathbf{M}_ℓ , we also consider the space-time Fourier modes

$$\varrho_\ell(\omega, \theta) := \chi(\omega) \varphi_\ell(\theta), \quad (\omega, \theta) \in [-\pi, \pi) \times \Theta_\ell, \quad (69)$$

in which χ is a spatial Fourier mode, and φ_ℓ is the temporal Fourier mode from (16):

$$\chi(\omega) := \exp\left(\frac{i\omega x}{h}\right), \quad \varphi_\ell(\theta) := \exp\left(\frac{i\theta t}{m^\ell \delta t}\right), \quad (x, t) \in \mathbf{M}_\ell. \quad (70)$$

The spatial frequency ω discretizes $[-\pi, \pi)$ with n_x points separated by a distance h , and, as previously, θ varies continuously in Θ_ℓ (defined in (17)). We refer to the smoothest Fourier modes on a given spatial mesh, that is, those with frequency $\omega = \mathcal{O}(h)$, as being *asymptotically smooth*.

Let $\lambda(\omega)$ and $\mu(\omega)$ be the Fourier symbols associated with spatial frequency ω of the fine- and coarse-grid time-stepping operators Φ and Ψ , respectively. Observe the slight change in notation from earlier sections: The eigenvalues $\lambda(\omega)$ and $\mu(\omega)$, and functions of them, are now described by the argument ω rather than with the subscript notation λ_i and μ_i . Then, the Fourier symbols $\tilde{A}_\ell(\omega, \theta)$ of A_ℓ are given by (see also (38))

$$\tilde{A}_0(\omega, \theta) = 1 - \lambda(\omega)e^{-i\theta}, \quad \tilde{A}_1(\omega, m\theta) = 1 - \mu(\omega)e^{-im\theta}. \quad (71)$$

The infinite-dimensional MGRIT error propagator \mathcal{E} in (7) can be block diagonalized, analogously to how it was first block diagonalized in space in Section 3.1, and then in time in Section 4. Specifically, under a similarity transform we have

$$\mathcal{E} \xrightarrow[\text{similarity transform}]{} \text{diag}_{(\omega, \theta) \in [-\pi, \pi) \times \Theta^{\text{low}}} \left(\hat{\mathcal{E}}(\omega, \theta) \right), \quad (72)$$

where, for a fixed frequency pair (ω, θ) , $\hat{\mathcal{E}}(\omega, \theta) \in \mathbb{C}^{m \times m}$ is the Fourier symbol associated with the m space-time modes (69) having frequencies $(\omega, \theta + \frac{2\pi p}{m})$, $p \in \{0, \dots, m-1\}$ (see Definition 1). The set of low frequencies Θ^{low} is as in (19).

The LFA theory from Section 4 can be used to compute the spectral radius of the diagonal blocks $\hat{\mathcal{E}}(\omega, \theta)$ as follows. Note that an analogous expression for the norm can be found, but the spectral radius is sufficient for our purposes.

Lemma 3 (Spectral radius of space-time error propagator). For a fixed pair of frequencies (ω, θ) , the spectral radius of the associated diagonal block in (72) is

$$\rho(\hat{\mathcal{E}}(\omega, \theta)) = |\lambda(\omega)|^{mv} \left| \frac{\tilde{A}_1(\omega, m\theta) - \tilde{A}_1^{\text{ideal}}(\omega, m\theta)}{\tilde{A}_1(\omega, m\theta)} \right|, \quad (\omega, \theta) \in [-\pi, \pi) \times \Theta^{\text{low}}, \quad (73)$$

with $\tilde{A}_1^{\text{ideal}}(\omega, m\theta) = 1 - [\lambda(\omega)]^m e^{-im\theta}$ the Fourier symbol of the coarse-grid space-time discretization that uses the ideal coarse-grid time-stepping operator $\Psi = \Phi^m$.

Proof. This follows directly from rearranging (62) of Corollary 2. \square

From (73), there are two mechanisms governing MGRIT convergence. First, the factor $|\lambda(\omega)|^{mv}$ arising from v sweeps of CF-relaxation in the pre-relaxation (recall Section 2.1). This mechanism will quickly damp error modes that rapidly decay under time-stepping, but will have little effect for error modes that decay slowly under time-stepping, when $|\lambda(\omega)| \approx 1$. Since MGRIT uses time-stepping as its local relaxation scheme, these modes must, instead, be targeted by the global coarse-grid correction, which corresponds to the second mechanism in (73). The effectiveness of this coarse-grid correction for a given space-time mode is determined by the corresponding *relative accuracy* of A_1 with respect to A_1^{ideal} . This realization allows us to draw a connection between the convergence of MGRIT for PDE (67) and classical spatial multigrid for steady-state advection-diffusion problems, as we now discuss.

Consider the steady-state advection-diffusion PDE $\mathcal{L}u := (\alpha_x, \alpha_y) \cdot \nabla u - \beta \Delta u = 0$ in two dimensions, with fine- and coarse-grid discretizations given by L_h and L_H , respectively. Here, (α_x, α_y) is a two-dimensional wave-speed, and $\beta \geq 0$ is the diffusivity. Let (ω_x, ω_y) be a two-component spatial Fourier frequency and consider the effect of coarse-grid correction on asymptotically smooth modes, i.e., $(\omega_x, \omega_y) = (\mathcal{O}(h), \mathcal{O}(h))$. Under reasonable assumptions on the relaxation scheme and the intergrid transfer operators, it can be shown that the two-grid convergence factor of an asymptotically smooth mode is proportional to^{39, 45}

$$\left| \frac{\tilde{L}_H(\omega_x, \omega_y) - \tilde{L}_h(\omega_x, \omega_y)}{\tilde{L}_H(\omega_x, \omega_y)} \right|, \quad (\omega_x, \omega_y) = (\mathcal{O}(h), \mathcal{O}(h)). \quad (74)$$

Notice that (74) closely resembles (73). For a given (ω_x, ω_y) , the fraction (74) determines the *relative accuracy* of L_H with respect to L_h , while its numerator determines the *absolute accuracy* of L_H with respect to L_h .³⁹

Suppose L_H is derived by rediscretizing L_h , then, since both L_H and L_h are consistent with \mathcal{L} , the numerator of (74) should be small as $(\omega_x, \omega_y) \rightarrow (0, 0)$. When $\beta \gg \mathcal{O}(h)$, so that L_h and L_H are close to elliptic, the denominator in (74) is typically some $\mathcal{O}(1)$ constant, independent of (ω_x, ω_y) . Thus, two-grid convergence is fast for all asymptotically smooth modes. However, in the

strongly non-elliptic case $\beta \rightarrow 0^+$ the denominator of (74) is not an $\mathcal{O}(1)$ constant independent of (ω_x, ω_y) . Instead, the denominator of (74) approximately vanishes for modes $(\alpha_x, \alpha_y) \cdot \left(\frac{\omega_x}{h}, \frac{\omega_y}{h}\right) \approx 0$, which are the so-called *characteristic components*.³⁹ Overall two-grid convergence is dramatically slowed by the inadequate coarse-grid correction of these components.

Characteristic components are Fourier modes that vary slowly—relative to the grid spacing—along the direction of characteristics (as defined by the advective component of the PDE), but that are free to vary in the direction normal to characteristics. Characteristic components that are also asymptotically smooth (as described above) are those which vary slowly also in the direction normal to characteristics. In the $\beta \rightarrow 0^+$ limit, on asymptotically smooth characteristic components, \tilde{L}_H vanishes up to small terms related to the truncation error of L_H , since L_H is a consistent discretization of \mathcal{L} , and $\tilde{\mathcal{L}}$ itself vanishes on these components. On non-characteristic components, \tilde{L}_H would typically be some $\mathcal{O}(1)$ constant. In other words, the relative accuracy of L_H on asymptotically smooth characteristic components is much less than that for all other asymptotically smooth components. The poor convergence of characteristic components in spatial multigrid was first described in Section 5.1 of Brandt,³⁴ is covered in great detail by Yavneh,³⁹ and has been discussed in many other contexts.^{37, 45–49}

Based on the resemblance of (73) to (74) and the above discussion, it is reasonable to expect that *if using a rediscritized coarse-grid operator, MGRIT convergence for discretizations of PDE (67) will deteriorate in the advection-dominated limit, at least in part, due to a poor coarse-grid correction of asymptotically smooth characteristic components*. Here we add the qualifier “at least in part” because there may also exist non-asymptotically smooth modes that are not efficiently damped by the solver (as numerical results in Section 6.3 will reveal). In the spatial, steady-state setting, when low-order discretizations are used, of all modes, only asymptotically smooth characteristic components are slow to converge, while the picture more complicated for higher-order discretizations (see Figure 4 of Oosterlee & Washio⁴⁶).

To make the above discussion on MGRIT convergence deterioration more precise: A_1 is a consistent space-time discretization of the PDE (67) up to some constant scaling factor, say, ζ , and, thus, its Fourier symbol for modes $\omega = \mathcal{O}(h)$ and $\theta = \mathcal{O}(\delta t)$ must be consistent with that of the continuous differential operator \mathcal{A} up to a scaling of ζ . Therefore, we have the Taylor expansion,

$$\tilde{A}_1(\omega, m\theta) \Big|_{\omega=\mathcal{O}(h)} = \zeta \tilde{\mathcal{A}}(\omega, m\theta) + \text{h.o.t} = i\zeta \left(\frac{\omega\alpha}{h} + \frac{m\theta}{m\delta t} \right) + \zeta\beta \frac{\omega^2}{h^2} + \text{h.o.t.} \quad (75)$$

Here, the higher-order terms arise from the truncation error of A_1 . Thus, the advective space-time component of $\tilde{\mathcal{A}}(\omega, m\theta)$ vanishes on space-time characteristic components; that is, in terms of modes (69), are those satisfying

$$(1, \alpha) \cdot \left(\frac{\theta}{\delta t}, \frac{\omega}{h} \right) = \frac{\theta}{\delta t} + \alpha \frac{\omega}{h} \approx 0 \quad \Rightarrow \quad \theta \approx -\frac{\omega\alpha\delta t}{h}. \quad (76)$$

For the discretization $\tilde{A}_1(\omega, m\theta)$, we therefore have

$$\tilde{A}_1 \left(\omega, m\theta \approx -\frac{\omega\alpha m\delta t}{h} \right) \Big|_{\omega=\mathcal{O}(h)} \approx \zeta\beta \frac{\omega^2}{h^2} + \text{h.o.t.} \quad (77)$$

Since $\omega = \mathcal{O}(h)$, the right-hand side of (77) will be bounded away from zero so long as β itself is. However, as $\beta \rightarrow 0^+$, the right-hand side of (77) vanishes up to terms related to the truncation error of A_1 , and the relative error factor in (73) may be large.

We emphasize that the result of Lemma 3 is a key distinguishing factor our LFA-based convergence theory from existing non-LFA MGRIT convergence theories.^{8, 31, 32} Specifically, since (73) retains both spatial and temporal Fourier information (results in References 8, 31, 32 retain only spatial Fourier information; see also Section 5), we have been able to compare it directly to fully Fourier-based convergence estimates developed in the spatial, steady-state setting, thereby showing that MGRIT convergence issues manifest for the same reasons as in the spatial setting.

6.2 | Semi-Lagrangian discretizations of linear advection

In this section, we investigate the general arguments made in the previous section as they apply specifically to semi-Lagrangian discretizations of the constant-wave-speed advection problem obtained by setting $\beta = 0$ in PDE (67). In De Sterck et al.,⁵¹ we consider a similar analysis for method-of-lines discretizations of advection problems that use finite-difference discretizations in space and Runge-Kutta temporal discretizations.

A general understanding of semi-Lagrangian discretizations for linear advection problems is useful for interpreting the results in this section, although it is not necessary. In essence, semi-Lagrangian methods approximate the solution at spatial mesh points at time $t_n + \delta t$ by integrating backwards along characteristics of the PDE to time t_n , and then approximating the PDE solution at the feet of these characteristics using polynomial interpolation (the feet of the characteristics do not, in general, intersect spatial mesh points, which is where the current approximation is known). Excellent introductions to these discretizations can

be found in References 54, 55, or, alternatively, see our previous works in References 15, 50 for the specific formulations we consider here. We write the time-stepping operator for a semi-Lagrangian discretization as $\Phi = S_p^{(\delta t)} \in \mathbb{R}^{n_x \times n_x}$, indicating that the discretization has a (global) order of accuracy $p \in \mathbb{N}$, and that it uses a time-step size of δt . Here, we consider only odd p , since in De Sterck et al.⁵⁰ we were able to develop efficient MGRIT solvers for odd p and not even p . The key distinction between odd and even p is whether the dominant term in the truncation error acts dissipatively or dispersively, respectively.⁵⁰ It is important to note that the calculations and results given here for odd p do not trivially extend to the case of even p , which have additional structure in a certain sense; we provide further details about this later.

We write the CFL number of the discretization $S_p^{(\delta t)}$ as $c := \frac{\alpha \delta t}{h} > 0$. A key quantity in our analysis here is the fractional part of the CFL number, which we denote by

$$\varepsilon^{(\delta t)} := \frac{\alpha \delta t}{h} - \left\lfloor \frac{\alpha \delta t}{h} \right\rfloor \in [0, 1). \quad (78)$$

We note that semi-Lagrangian discretizations for this linear advection problem are unconditionally stable with respect to c . However, the discretizations admit a form of translational symmetry in c that means it will only be necessary for us to study MGRIT convergence for $c \in (0, 1]$.¹ For this reason, we also sometimes abuse notation by referring to $\varepsilon^{(\delta t)}$ as the fine-grid CFL number. From Krzysik¹⁵ p. 103, note that the fractional component of the coarse-grid CFL number satisfies $\varepsilon^{(m\delta t)} := \frac{\alpha m \delta t}{h} - \left\lfloor \frac{\alpha m \delta t}{h} \right\rfloor = m\varepsilon^{(\delta t)} - \lfloor m\varepsilon^{(\delta t)} \rfloor \in [0, 1)$. This brings us to the following key assumption needed in the forthcoming analysis.

Assumption 3. The fine-grid CFL number $c := \frac{\alpha \delta t}{h}$ is not an integer, and, furthermore, it is such that the associated coarse-grid CFL number of $m\varepsilon$ is not an integer. In other words, the domain of $\varepsilon^{(\delta t)}$ in (78) is restricted as

$$\varepsilon^{(\delta t)} \in \Upsilon_m := (0, 1) \setminus \{\varepsilon : m\varepsilon - \lfloor m\varepsilon \rfloor = 0\}. \quad (79)$$

The reason for this assumption is that if the CFL number is an integer, then characteristics intersect with the mesh, and all eigenvalues of the associated semi-Lagrangian discretization have unit magnitude, which is not covered by our LFA theory as per Assumption 2.

With notation and assumptions now specified, we present our two results for this section. First, Theorem 4 confirms that asymptotically smooth characteristic components do receive a poor coarse-grid correction compared to all other asymptotically smooth modes. Second, Theorem 5 shows that this poor coarse-grid correction prevents the possibility of robust two-grid convergence with respect to problem parameters.

Theorem 4 (Order zero coarse-grid correction). Suppose $\Phi = S_p^{(\delta t)}$, and $\Psi = S_p^{(m\delta t)}$, with p odd. Suppose that Assumption 3 holds. Then, asymptotically smooth Fourier modes receive a coarse-grid correction that is order $p+1$ small in ω if they are not characteristic components, while asymptotically smooth characteristic components receive an order zero coarse-grid correction in ω ,

$$\frac{\left| \tilde{A}_1(\omega, m\theta) - \tilde{A}_1^{\text{ideal}}(\omega, m\theta) \right|}{\left| \tilde{A}_1(\omega, m\theta) \right|} \bigg|_{\omega=\mathcal{O}(h)} = \begin{cases} \mathcal{O}(\omega^{p+1}), & \theta \not\approx -\frac{\omega \alpha \delta t}{h}, \\ \mathcal{O}(1), & \theta \approx -\frac{\omega \alpha \delta t}{h}. \end{cases} \quad (80)$$

Proof. This proof works by estimating the numerator and denominator of (80) for asymptotically smooth Fourier modes by using the semi-Lagrangian eigenvalue estimates developed in Appendix D.1.

We first consider the square of the numerator in (80). From (71), recall $\tilde{A}_1(\omega, m\theta) = 1 - \mu(\omega)e^{-im\theta}$ and, from Lemma 3, $\tilde{A}_1^{\text{ideal}}(\omega, m\theta) = 1 - [\lambda(\omega)]^m e^{-im\theta}$. Since $\Psi = S_p^{(m\delta t)}$, we take $\mu(\omega) = s_p^{(m\delta t)}(\omega)$, the eigenvalue of the coarse-grid semi-Lagrangian discretization, which we will estimate using (D60). Since $\Phi = S_p^{(\delta t)}$, we take $[\lambda(\omega)]^m = [s_p^{(\delta t)}(\omega)]^m$, for which we directly use the estimate of (D61). The square of the numerator of (80) then becomes

$$\left| \tilde{A}_1(\omega, m\theta) - \tilde{A}_1^{\text{ideal}}(\omega, m\theta) \right|^2 = \left| s_p^{(m\delta t)}(\omega) - [s_p^{(\delta t)}(\omega)]^m \right|^2 \quad (81)$$

$$= \left| \exp\left(-\frac{i\omega \alpha m \delta t}{h}\right) \right|^2 \left| \left[f_{p+1}(\varepsilon^{(m\delta t)}) - m f_{p+1}(\varepsilon^{(\delta t)}) \right] d_{p+1}(\omega) + \mathcal{O}(\omega^{p+2}) \right|^2. \quad (82)$$

¹If p is odd, and $S_p^{(\delta t)}$ is a discretization for some CFL number $c = \hat{c} \in (0, 1]$, then the discretization for the CFL number $c = \hat{c} + k$, $k \in \mathbb{N}$, can be written as $L^{(k)} S_p^{(\delta t)}$, where $L^{(k)} \in \mathbb{R}^{n_x \times n_x}$ is a circulant matrix with ones on its k th subdiagonal. Note that $[L^{(k)} S_p^{(\delta t)}]^m = L^{(mk)} [S_p^{(\delta t)}]^m$. Analogously, if $S_p^{(m\delta t)}$ is the rediscritized operator (i.e., the discretization for CFL number $m\hat{c}$), then the discretization for the CFL number $m(\hat{c} + k) = m\hat{c} + mk$ can be written as $L^{(mk)} S_p^{(m\delta t)}$. Multiplication by $L^{(mk)}$ causes a rotation of eigenvalues, but not a change in their magnitude. Applying this fact to, for example, $\rho(\mathcal{E}_i)$ in Corollary 2, it is easy to see that MGRIT convergence is independent of k .

Now substitute $d_{p+1}(\omega) = (-1)^{\frac{p+1}{2}} \omega^{p+1} + \mathcal{O}(\omega^{p+2})$, as per (D65), and then simplify to give

$$\left| \tilde{A}_1(\omega, m\theta) - \tilde{A}_1^{\text{ideal}}(\omega, m\theta) \right|^2 = \left(\omega^{p+1} \left[f_{p+1}(\varepsilon^{(m\delta t)}) - m f_{p+1}(\varepsilon^{(\delta t)}) \right] \right)^2 (1 + \mathcal{O}(\omega)). \quad (83)$$

Thus, from (83), the numerator of (80) satisfies

$$\left| \tilde{A}_1(\omega, m\theta) - \tilde{A}_1^{\text{ideal}}(\omega, m\theta) \right| = \omega^{p+1} \check{C}_1 + \mathcal{O}(\omega^{p+2}), \quad (84)$$

for asymptotically smooth Fourier modes, with \check{C}_1 some positive constant.

We now consider the square of the denominator in (80). To do so, we again take $\mu(\omega) = s_p^{(m\delta t)}(\omega)$, which we will estimate by appealing to (D60), to give

$$\left| \tilde{A}_1(\omega, m\theta) \right|^2 = \left| 1 - s_p^{(m\delta t)}(\omega) e^{-im\theta} \right|^2, \quad (85)$$

$$= \left| 1 - \exp \left(\underbrace{-im \left[\theta + \frac{\omega \alpha \delta t}{h} \right]}_{=: \eta} \right) \left(1 - \underbrace{f_{p+1}(\varepsilon^{(m\delta t)}) d_{p+1}(\omega) + \mathcal{O}(\omega^{p+2})}_{=: \xi} \right) \right|^2, \quad (86)$$

$$= \left| 1 - (1 - \xi) \cos \eta + i(1 - \xi) \sin \eta \right|^2 = 2(1 - \cos \eta)(1 - \xi) + \xi^2. \quad (87)$$

Now apply $d_{p+1}(\omega) = (-1)^{\frac{p+1}{2}} \omega^{p+1} + \mathcal{O}(\omega^{p+2})$, as per (D65), to write $1 - \xi = 1 + \mathcal{O}(\omega^{p+1})$, and $\xi^2 = \left(\omega^{p+1} f_{p+1}(\varepsilon^{(m\delta t)}) \right)^2 (1 + \mathcal{O}(\omega))$. This gives the the following estimate

$$\left| \tilde{A}_1(\omega, m\theta) \right|^2 = 2 \left[1 - \cos \left(m \left[\theta + \frac{\omega \alpha \delta t}{h} \right] \right) \right] \left(1 + \mathcal{O}(\omega^{p+1}) \right) + \left(\omega^{p+1} f_{p+1}(\varepsilon^{(m\delta t)}) \right)^2 (1 + \mathcal{O}(\omega)). \quad (88)$$

Thus, for asymptotically smooth modes, the denominator of (80) satisfies

$\left| \tilde{A}_1 \left(\omega, m\theta \approx -\frac{\omega \alpha m \delta t}{h} \right) \right| = \check{C}_2 + \mathcal{O}(\omega)$, and $\left| \tilde{A}_1 \left(\omega, m\theta \approx -\frac{\omega \alpha m \delta t}{h} \right) \right| \geq \check{C}_3 \omega^{p+1}$ for some positive constants \check{C}_2, \check{C}_3 . Using this in combination with (84) gives the claimed result of (80). \square

Remark 3. Additional structure for dispersive discretizations. We briefly mentioned earlier that our results for even orders p do not trivially follow from those for odd orders p . If p is even, then the first term in the truncation error of the discretization is imaginary, rather than real as when p is odd; specifically, the $d_{p+1}(\omega)$ symbol in (86) is imaginary. The significance of this is that the symbol of the continuous differential operator is imaginary also, and, so, there exist characteristic components for which the symbol of the continuous differential operator cancels the first truncation error term. That is, if we denote these modes by $\theta = \theta_*(\omega)$, then we have $\left| \tilde{A}_1(\omega, m\theta_*(\omega)) \right| = \mathcal{O}(\omega^{p+2})$. Following through the details of the above proof, we see that the coarse-grid correction for these modes is $\mathcal{O}(\omega^{-1})$, meaning that they are blown up by the solver. It is unclear, however, to what extent, if any, these modes are present in simulations of the initial-value problem for finite n_t , or whether they only occur for the time-periodic problem in the limit of $n_t \rightarrow \infty$. For example, initial experiments suggest that such modes may only arise for initial-value problems that are much more resolved in time than in space. In any event, this insight is interesting, and it possibly has a connection with why the approaches in De Sterck et al.⁵⁰ did not prove successful for dispersive discretizations. We leave more detailed study of this topic for future work.

One might anticipate that the poor coarse-grid correction of characteristic components described in Theorem 4 impairs overall two-grid convergence, destroying the possibility of fast convergence. For example, in the spatial, steady-state case, the poor coarse-grid correction of asymptotically smooth characteristic components leads to a two-grid convergence factor of one half when using a basic discretization and standard multigrid components.^{34, 39, 45} Indeed, Theorem 5 below shows that, if rediscretizing the semi-Lagrangian method on the coarse grid, MGRIT convergence is not robust with respect to CFL number or coarsening factor, with the two-grid convergence factor $\max_{(\omega, \theta) \in [-\pi, \pi) \times \Theta^{\text{low}}} \rho(\hat{\mathcal{E}}(\omega, \theta))$ being significantly larger than unity for certain combinations of these parameters. This is consistent with our previous numerical results in References 15, 50, where MGRIT often diverged for such problems. Recall that in $\mathcal{O}(n_t/m)$ iterations MGRIT converges to the exact solution by sequentially propagating the initial condition across the time domain—something not captured by our LFA estimate of the spectral radius (see the end of Section 5). The aforementioned “divergence”—which is captured by the LFA estimate—is that occurring on these “middle iterations” before the local relaxation scheme has any significant global impact on convergence. Finally, note that although the context is different, the below theorem is also consistent with the numerical results reported in the final paragraph

of Section 6.3.2 of Schmitt et al.,¹⁹ wherein Parareal convergence degraded substantially in the hyperbolic limit of a nonlinear advection-diffusion problem when using a semi-Lagrangian discretization on the coarse grid and $m = \mathcal{O}(10^4)$.

Theorem 5 (Convergence factor lower bound). Suppose $\Phi = S_p^{(\delta t)}$, and $\Psi = S_p^{(m\delta t)}$, with p odd. Suppose that Assumption 3 holds. Then, over all space-time Fourier modes, the MGRIT spectral radius (73) satisfies the following lower bound independent of the number of CF-relaxations ν ,

$$\max_{(\omega, \theta) \in [-\pi, \pi] \times \Theta^{\text{low}}} \rho(\hat{\mathcal{E}}(\omega, \theta)) \geq \check{\rho}_p(\varepsilon^{(\delta t)})(1 + \mathcal{O}(h)), \quad (89)$$

where,

$$\check{\rho}_p(\varepsilon^{(\delta t)}) := m \frac{f_{p+1}(\varepsilon^{(\delta t)})}{f_{p+1}(\varepsilon^{(m\delta t)})} - 1, \quad \varepsilon^{(\delta t)} \in \Upsilon_m, \quad (90)$$

with f_{p+1} the degree $p+1$ polynomial defined in (D59).

Furthermore, $\check{\rho}_p(\varepsilon^{(\delta t)})$ is larger than unity for an interval of fine-grid CFL numbers $\varepsilon^{(\delta t)}$ that quickly covers Υ_m in (79) as m increases. More precisely, for $m \geq 2$,

$$\check{\rho}_p(\varepsilon^{(\delta t)}) > 1 \quad \text{when} \quad \varepsilon^{(\delta t)} \in \Upsilon_m \cap \left(\frac{2}{3m}, 1 - \frac{2}{3m} \right). \quad (91)$$

Proof. Since asymptotically smooth characteristic components represent only a subset of all Fourier modes, we immediately get the following lower bound on the worst-case spectral radius in (73)

$$\max_{(\omega, \theta) \in [-\pi, \pi] \times \Theta^{\text{low}}} \rho(\hat{\mathcal{E}}(\omega, \theta)) \geq \rho\left(\hat{\mathcal{E}}\left(\omega, \theta = -\frac{\omega \alpha \delta t}{h}\right)\right) \Big|_{\omega = \mathcal{O}(h)}. \quad (92)$$

Now we evaluate the (square of the) right-hand side of this equation. First, consider the factor $|\lambda(\omega)|^{m\nu}$ in the spectral radius (73) that arises from $\nu \in \mathbb{N}_0$ sweeps of CF-relaxation. Invoking the eigenvalue estimate for the ideal coarse-grid operator from (D61), we have for asymptotically smooth Fourier modes

$$|\lambda(\omega)|^{m\nu} = \left| [s_p^{(\delta t)}(\omega)]^m \right|^\nu = \left| \exp\left(-\frac{i\omega \alpha m \delta t}{h}\right) \right|^\nu \left| 1 + \mathcal{O}(\omega^{p+1}) \right|^\nu = 1 + \mathcal{O}(h^{p+1}). \quad (93)$$

Notice that, as described in the previous section, this relaxation effectively does nothing for the convergence of asymptotically smooth Fourier modes.

Thus, by invoking the numerator (83), and the denominator (88), the square of the right-hand side of (92) is

$$\rho^2\left(\hat{\mathcal{E}}\left(\omega, \theta = -\frac{\omega \alpha \delta t}{h}\right)\right) \Big|_{\omega = \mathcal{O}(h)} = \left[1 + \mathcal{O}(h^{p+1})\right]^2 \frac{\left(\omega^{p+1} \left[f_{p+1}(\varepsilon^{(m\delta t)}) - m f_{p+1}(\varepsilon^{(\delta t)})\right]\right)^2 (1 + \mathcal{O}(h))}{\left(\omega^{p+1} f_{p+1}(\varepsilon^{(m\delta t)})\right)^2 (1 + \mathcal{O}(h))}, \quad (94)$$

$$= \left(m \frac{f_{p+1}(\varepsilon^{(\delta t)})}{f_{p+1}(\varepsilon^{(m\delta t)})} - 1\right)^2 \frac{1 + \mathcal{O}(h)}{1 + \mathcal{O}(h)} = \left(\check{\rho}_p(\varepsilon^{(\delta t)})\right)^2 \frac{1 + \mathcal{O}(h)}{1 + \mathcal{O}(h)}. \quad (95)$$

Next, use the geometric expansion $\frac{1 + \mathcal{O}(h)}{1 + \mathcal{O}(h)} = 1 + \mathcal{O}(h)$, then take the square root of both sides of (95) and apply that $\sqrt{1 + \mathcal{O}(h)} = 1 + \mathcal{O}(h)$. Plugging the result into (92) gives the claimed result of (89). When taking the square root of (95), note that $\check{\rho}_p(\varepsilon^{(m\delta t)}) > 0$ for all $\varepsilon^{(\delta t)} \in \Upsilon_m$, which follows by combining $|m f_{p+1}(\varepsilon^{(\delta t)})| > |f_{p+1}(\varepsilon^{(m\delta t)})|$ (see Krzysik¹⁵ Lemma 4.4), and $\text{sign}(f_{p+1}(\varepsilon^{(m\delta t)})) = \text{sign}(m f_{p+1}(\varepsilon^{(\delta t)}))$ (see Krzysik¹⁵ Lemma B.1). The remainder of the proof regarding when $\check{\rho}_p > 1$ is technical and can be found in Appendix E. \square

Note that there may also exist $\varepsilon^{(\delta t)} \in \Upsilon_m$ outside of the interval considered in (91) for which $\check{\rho}_p(\varepsilon^{(\delta t)}) > 1$; see Figure 2. However, this interval is sufficient for demonstrating our primary point which is that the interval of $\varepsilon^{(\delta t)}$ for which $\check{\rho}_p(\varepsilon^{(\delta t)}) > 1$ quickly covers Υ_m as m grows.

6.3 | Numerical results

In this section, we present numerical results to support the general arguments made in Section 6.1 on MGRIT convergence and characteristic components, and those specific to semi-Lagrangian schemes made in Section 6.2. In Figure 1 a visual picture of

what is described in Sections 6.1 and 6.2 is given. Specifically, for the order $p = 3$ semi-Lagrangian discretization, we arbitrarily pick a CFL number of $c = 0.8$ and coarsening factor of $m = 4$, and plot in Fourier space the key quantities from Lemma 3 governing MGRIT convergence for this problem. To make the contour plots, we sample $\omega \in [-\pi, \pi)$ with 1024 points, and $\theta \in \Theta^{\text{low}}$ with $1024/m$ points.

First, consider the absolute error of the coarse-grid discretization, which is shown in the top left panel of Figure 1. This quantity is small for $\omega \approx 0$, arising from the fact that both A_1 and A_1^{ideal} are consistent with the continuous differential operator \mathcal{A} from (67) as $\omega \rightarrow 0$ and, thus, are consistent with one another in this regime. Next, consider the magnitude of the coarse-grid symbol, which is shown in the top right panel of Figure 1. In this plot, we overlay with dashed green lines characteristic components with frequency $\theta = -\frac{\omega \alpha \delta t}{h}$. As expected, the symbol approximately vanishes for asymptotically smooth characteristic components (with $\omega \approx 0$), but is bounded away from zero for all other asymptotically smooth components. Again, this occurs since A_1 is consistent with \mathcal{A} as $\omega \rightarrow 0$, and \mathcal{A} vanishes on characteristic components. Notice that even for some non-asymptotically smooth characteristic components, that is, $\theta \approx -\frac{\omega \alpha \delta t}{h}$ with $\omega \gg \mathcal{O}(h)$, this symbol appears to approximately vanish.

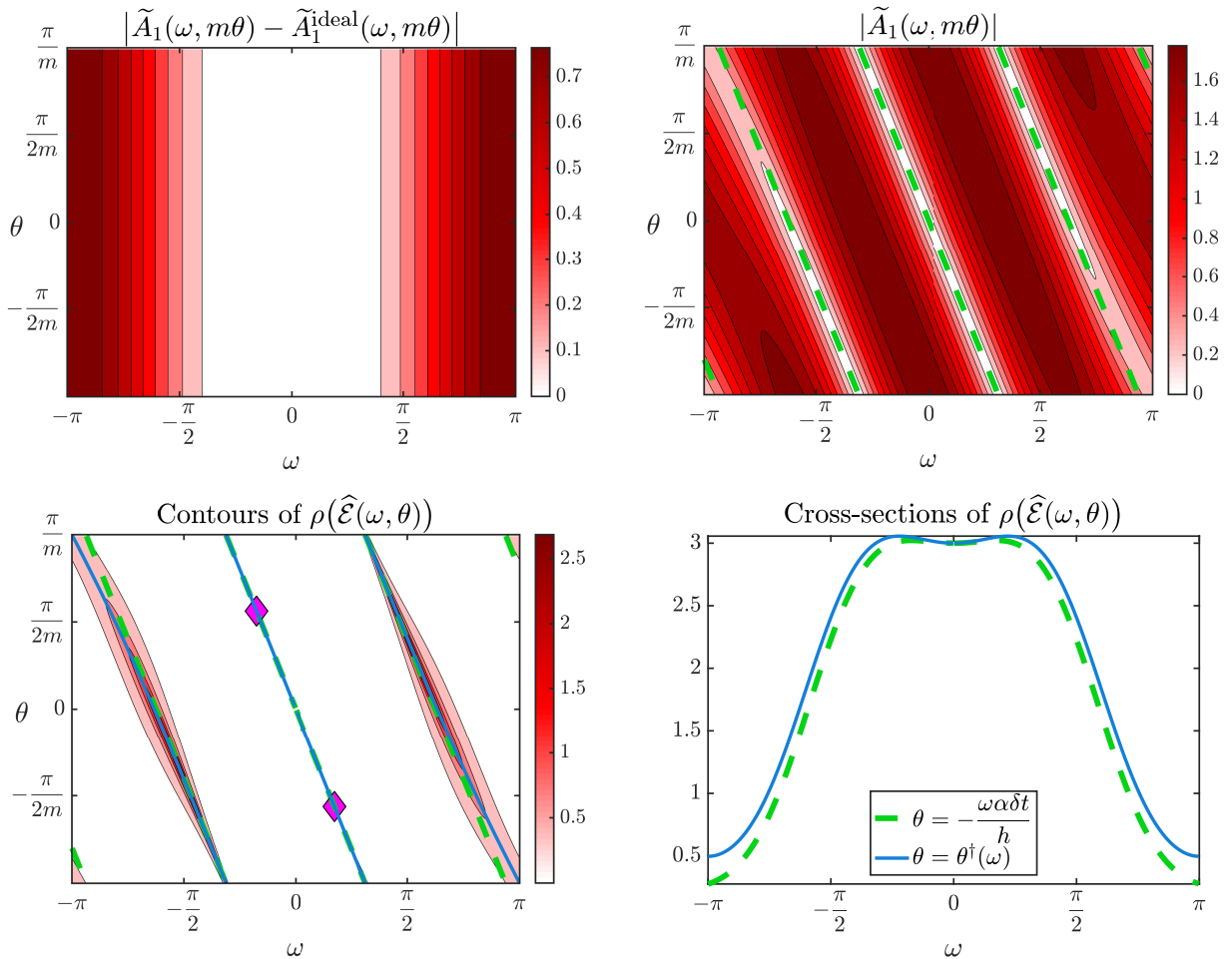


FIGURE 1 Plots in Fourier frequency space of quantities relating to the LFA spectral radius in Lemma 3 for a $p = 3$ semi-Lagrangian discretization of linear advection using rediscretization on the coarse grid. The coarsening factor is $m = 4$, FCF-relaxation is used, and the CFL number is $c = 0.8$. Top left: Difference between symbols of coarse-grid operator and ideal coarse-grid operator. Top right: Symbol of coarse-grid operator. Bottom left: Contour of spectral radius evaluated with 1024 points in ω and $1024/m$ points in θ , with its maxima over the whole space marked with magenta diamonds. Bottom right: Cross-sections of the spectral radius along the green and blue lines pictured in the bottom left panel. Dashed green lines mark characteristic components with frequency $\theta(\omega) = -\frac{\omega \alpha \delta t}{h}$, while blue lines mark the slowest converging modes $\theta(\omega) = \theta^\dagger(\omega) = \frac{1}{m} \arg \mu(\omega)$ (see Theorem 3).

Next, consider the spectral radius itself, which is shown in the bottom row of Figure 1, beginning with the contours shown in the left panel. On this plot, we again overlay characteristic components, and we also overlay with blue lines the set of slowest converging modes $\theta = \theta^*(\omega)$ as given in Theorem 3. Not surprisingly, the spectral radius is large where $|\tilde{A}_1|$ approximately vanishes. As reflected by the green lines overlapping with the blue lines, it appears that for temporally smooth components, with $\omega \approx 0$, the convergence is poorest for the characteristic components. In fact, *all modes with $\omega \approx 0$ are rapidly damped except those that are characteristic components*; it is not particularly obvious from this plot, however, what the value of the function is along the green and blue lines. Therefore, we plot the values of $\rho(\hat{\mathcal{E}}(\omega, \theta))$ along these green and blue lines in the bottom right panel of Figure 1. From the bottom right panel, it becomes apparent that smooth characteristic components having $\theta = -\frac{\omega \alpha \delta t}{h}$ do indeed diverge, with $\rho \approx 3 > 1$ for these modes. Finally, notice that, while convergence is certainly poor for asymptotically smooth characteristic components, convergence is poor also for many characteristic components which are not asymptotically smooth. This is an example of why we say that poor MGRIT convergence stems *at least in part* from the poor coarse-grid correction of asymptotically smooth characteristic components.

We now provide numerical evidence that the LFA spectral radius of MGRIT on infinite time domains given in Corollary 2 is an accurate predictor of the effective MGRIT convergence factor on finite time domains, and we also provide numerical verification of its lower bound given in Theorem 5. Figure 2 shows effective and LFA MGRIT convergence factors as a function of the CFL number for semi-Lagrangian schemes of orders $p = 1, 3$ (note that the quantities shown in Figure 2 are symmetric over $\epsilon^{(\delta t)} \in (0, 1)$, so, to better highlight the details we show them only for $\epsilon^{(\delta t)} \in (\frac{1}{2}, 1)$). The thin solid lines in the plots are the worst-case LFA convergence factor $\max_{(\omega, \theta) \in [-\pi, \pi) \times \Theta^{\text{low}}} \rho(\hat{\mathcal{E}}(\omega, \theta))$, which we evaluate by discretizing ω with 2^7 points. Circle markers overlaid on the plots are numerical data from Figure 2 of De Sterck et al.,⁵⁰ and correspond to convergence factors measured on final MGRIT iterations before stopping criteria are reached and, thus, represent effective MGRIT convergence factors for a finite interval $t \in (0, T]$. These MGRIT tests used a uniformly random initial iterate, and a space-time domain discretized with $n_x \times n_t = 2^7 \times 2^{15}$ points. First, notice that the LFA MGRIT convergence factor provides a very good approximation to the experimentally measured effective convergence factors. Second, notice that convergence is not robust for these problems, with the solver diverging for most combinations of m and c , as indicated by the convergence factor being larger than unity.

Also shown in Figure 2 as the thick dashed lines is the lower bound on the LFA estimate of the spectral radius (thin solid lines) given in Theorem 5. This lower bound appears very tight, essentially sitting on top of the LFA estimate in the $p = 1$ case. This suggests for $p = 1$ that it is indeed the inadequate coarse-grid correction of asymptotically smooth characteristic components

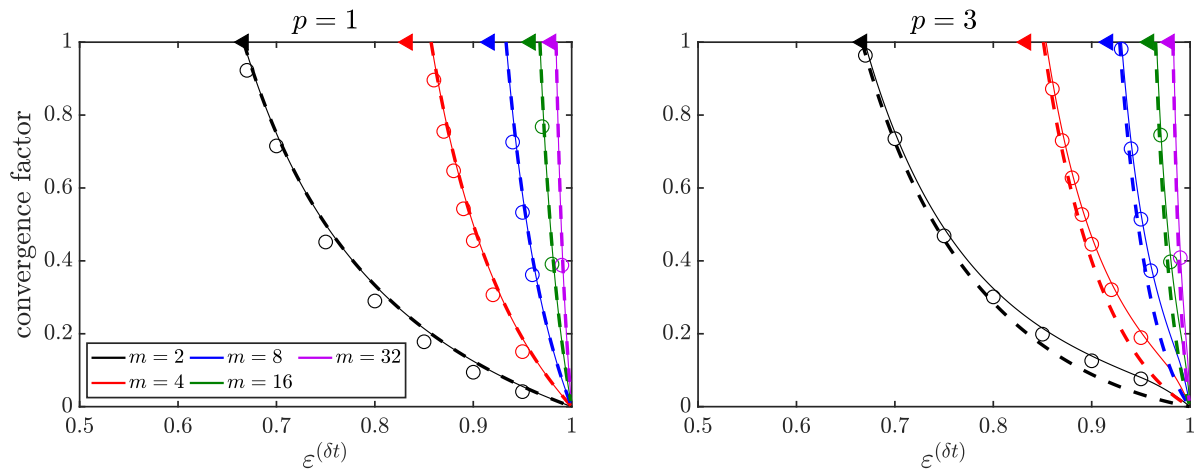


FIGURE 2 Numerical confirmation of Theorem 5: Convergence factors for the semi-Lagrangian discretizations $\Phi = S_p^{(\delta t)}$, with $p = 1$ (left), and $p = 3$ (right), as a function of fractional fine-grid CFL number $\epsilon^{(\delta t)}$ when rediscretizing on the coarse grid, $\Psi = S_p^{(m\delta t)}$. MGRIT uses FCF-relaxation ($\nu = 1$), and a coarsening factor of m . Thin solid lines are the LFA convergence factor $\max_{(\omega, \theta) \in [-\pi, \pi) \times \Theta^{\text{low}}} \rho(\hat{\mathcal{E}}(\omega, \theta))$ obtained by discretizing ω with 128 points. Thick dashed lines are the function $\check{\rho}_p(\epsilon^{(\delta t)})$ from (90) that acts as a lower bound on the LFA convergence factor (see (89)). Filled triangle markers are $\epsilon^{(\delta t)} = 1 - \frac{2}{3m}$, the right-hand end point of the interval in (91) on which $\check{\rho}_p(\epsilon^{(\delta t)})$ is shown to exceed unity. Open circle markers are experimentally measured effective convergence factors of MGRIT on a finite interval $t \in (0, T]$ taken from Figure 2 of De Sterck et al.⁵⁰

described in Theorem 4 that determines the overall two-grid convergence factor, at least for problems with convergence factors visible in the plot (i.e., those less than one). In contrast, the lower bound is slightly less tight in the $p = 3$ case, suggesting that it is not always these modes that determine overall two-grid performance. This is consistent with what is shown in the example in the bottom right panel of Figure 1. Nevertheless, the lower bound from Theorem 5 does accurately capture the interval for which the overall two-grid convergence factor exceeds unity, and it is clearly capable of demonstrating in the process that MGRIT convergence is not robust for this problem with respect to either m or c .

6.4 | Improved coarse-grid operators

Slow convergence of characteristic components has been widely studied in the spatial multigrid case, and, so, it is useful to consider the solutions proposed there, and to understand to what extent they can be applied in the MGRIT context. While several potential fixes have been proposed, for which detailed summaries can be found in Section 5 of Yavneh³⁹ and Section 7 of Trottenberg et al.,³⁷ it is important to note that none appear to yield multigrid convergence that is as efficient and robust as that for elliptic problems in general.

One proposed remedy is to use so-called downstream relaxation,^{37, 39, 56, 57} which essentially amounts to carrying out relaxation in an order that propagates errors and/or residuals downstream, along characteristics. But unfortunately, in the multigrid-in-time context considered here, downstream relaxation is nothing more than sequential time-stepping, the exact procedure that we are trying to avoid! Other ideas considered include residual overweighting,⁴⁵ and accelerating multigrid convergence using a Krylov method.⁴⁶

Considering (74), arguably the most effective way to improve convergence for smooth characteristic components is to increase the absolute accuracy of the coarse-grid operator with respect to the fine-grid operator. To do this, the coarse-grid operator needs to be designed so that its truncation error better approximates that of the fine-grid operator, at least for smooth characteristic components. This key idea was first introduced in Yavneh,³⁹ and was also later considered by Bank et al.⁴⁸ In the MGRIT context, that is, Lemma 3, this amounts to modifying the coarse-grid time-stepping operator so that its truncation error better approximates that of the ideal coarse-grid operator. An idea related to this was explored in Danieli & MacLachlan⁵⁸ for explicit temporal discretizations of nonlinear hyperbolic PDEs, where Ψ was directly constructed to match terms in a Taylor expansion of Φ^m , though stability issues limit that approach to very small fine-grid CFL numbers. A similar idea was also recently used by Vargas et al.⁵⁹ to develop effective MGRIT coarse-grid operators for chaotic problems, including the Lorentz system and the Kuramoto–Sivashinsky equation.

This idea of approximately matching truncation errors formed the basis of our recent works in References 50–52. Perhaps the most relevant of these works to the present context is De Sterck et al.,⁵⁰ where we designed very effective MGRIT coarse-grid operators for semi-Lagrangian discretizations of variable-wave-speed linear advection problems in multiple space dimensions. The coarse-grid operators in De Sterck et al.⁵⁰ consist of first applying a rediscretized coarse-grid operator, followed by a truncation error correction, which has to be applied in an implicit sense (i.e., it requires a linear solve) to ensure stability. In fact, the following theorem confirms that the coarse-grid operator from equation (3.20) of De Sterck et al.⁵⁰ does provide a better coarse-grid correction for asymptotically smooth characteristic components than rediscretization does, as considered in Theorem 4. Furthermore, the fact that this coarse-grid operator yields fast and robust convergence for all modes can be seen from results in Figure 3 of De Sterck et al.,⁵⁰ which plots the LFA spectral radius of MGRIT, analogous to those plots in Figure 2 for rediscretization.

Theorem 6 (Improved coarse-grid correction). Suppose $\Phi = S_p^{(\delta t)}$, with p odd. Further, suppose that $\Psi = \left(I - [f_{p+1}(\varepsilon^{(m\delta t)}) - mf_{p+1}(\varepsilon^{(\delta t)})]D_{p+1} \right)^{-1} S_p^{(m\delta t)}$, where f_{p+1} is as in (D59), $\varepsilon^{(\delta t)}$ is as in (78), and D_{p+1} is as explained in Appendix D.1. Suppose the fine-grid CFL number is not an integer. Then, asymptotically smooth Fourier modes receive a coarse-grid correction that is order $p+2$ small in ω if they are not characteristic components, while asymptotically smooth characteristic components receive an order one coarse-grid correction in ω ,

$$\left| \frac{\tilde{A}_1(\omega, m\theta) - \tilde{A}_1^{\text{ideal}}(\omega, m\theta)}{\tilde{A}_1(\omega, m\theta)} \right| \bigg|_{\omega=\mathcal{O}(h)} = \begin{cases} \mathcal{O}(\omega^{p+2}), & \theta \not\approx -\frac{\omega\alpha\delta t}{h}, \\ \mathcal{O}(\omega), & \theta \approx -\frac{\omega\alpha\delta t}{h}. \end{cases} \quad (96)$$

Proof. This proof proceeds analogously to that of Theorem 4. We first consider the square of the denominator in (96). For eigenvalue estimates of Ψ we use (D66) of Lemma 7 to obtain

$$\begin{aligned} \left| \tilde{A}_1(\omega, m\theta) \right|^2 &= 2 \left[1 - \cos \left(m \left[\theta + \frac{\omega \alpha \delta t}{h} \right] \right) \right] \left(1 + \mathcal{O}(\omega^{p+1}) \right) \\ &\quad + \left(\omega^{p+1} m f_{p+1}(\varepsilon^{(\delta t)}) \right)^2 \left(1 + \mathcal{O}(\omega) \right). \end{aligned} \quad (97)$$

Just as in Theorem 4, we have for asymptotically smooth modes that

$$\left| \tilde{A}_1 \left(\omega, m\theta \approx -\frac{\omega \alpha m \delta t}{h} \right) \right| = \check{C}_4 + \mathcal{O}(\omega), \text{ and } \left| \tilde{A}_1 \left(\omega, m\theta \approx -\frac{\omega \alpha m \delta t}{h} \right) \right| \geq \check{C}_5 \omega^{p+1} \text{ for some positive constants } \check{C}_4, \check{C}_5.$$

Now consider the square of the numerator in (96). For eigenvalue estimates of the ideal coarse-grid operator we use (D61), and for Ψ we again use (D66). This gives

$$\begin{aligned} \left| \tilde{A}_1(\omega, m\theta) - \tilde{A}_1^{\text{ideal}}(\omega, m\theta) \right|^2 &= \left| \exp \left(-\frac{i\omega \alpha m \delta t}{h} \right) \right|^2 \left| \left(1 - m f_{p+1}(\varepsilon^{(\delta t)}) d_{p+1}(\omega) + \mathcal{O}(\omega^{p+2}) \right) \right. \\ &\quad \left. - \left(1 - m f_{p+1}(\varepsilon^{(\delta t)}) d_{p+1}(\omega) + \mathcal{O}(\omega^{p+2}) \right) \right|^2. \end{aligned} \quad (98)$$

For all asymptotically smooth Fourier modes we have $\left| \tilde{A}_1(\omega, m\theta) - \tilde{A}_1^{\text{ideal}}(\omega, m\theta) \right| = \mathcal{O}(\omega^{p+2})$; combining this with the above result for $\left| \tilde{A}_1(\omega, m\theta) \right|$ results in (96). \square

7 | CONCLUSIONS

We have developed an LFA convergence theory for the two-level iterative parallel-in-time method MGRIT, which also applies to the Parareal method. The theory is presented in closed form, with analytical expressions for the LFA results for the norm and spectral radius of MGRIT applied to infinite time domains, approximating the effective convergence factor of MGRIT on finite time domains. Final convergence results from our LFA theory closely resemble several existing results from the literature that were derived via alternate means; however, our LFA framework is uniquely placed to shed light on the poor convergence of MGRIT for advection-dominated problems when using the standard approach of rediscrctizing on the coarse grid. In essence, this is because our theory can be used to describe convergence of space-time Fourier modes, allowing for straightforward comparison with existing Fourier-based analyses in the spatial, steady-state multigrid setting used to describe convergence issues there.^{34, 39}

We find that when using a rediscrctized coarse-grid operator for MGRIT, convergence issues arise that are due, at least in part, to an inadequate coarse-grid correction of a subset of asymptotically smooth Fourier modes known as characteristic components. It is well known that an inadequate coarse-grid correction of these same modes also gives rise to poor convergence for spatial multigrid methods when applied to steady-state advection-dominated problems. For a class of semi-Lagrangian discretizations of linear advection problems, we prove that this inadequate coarse-grid correction precludes robust MGRIT convergence when using rediscrctization on the coarse grid. In De Sterck et al.,⁵¹ we again use this framework to investigate MGRIT convergence for classical method-of-lines type discretizations of advection problems.

Leveraging this connection to the understanding of slow convergence for spatial multigrid solvers is key to developing improved parallel-in-time solvers for advection-dominated problems, by generalizing to the MGRIT setting techniques used to improve convergence. This approach has already proven successful in our work for semi-Lagrangian discretizations⁵⁰ and, also for method-of-lines discretizations for both linear advection equations,⁵¹ and for nonlinear hyperbolic PDEs with shocks.⁵²

One direction for future work is to extend the closed-form LFA theory developed here to the case of three-level MGRIT, to better understand the impacts of inexact coarse-grid solves on characteristic components. Another possible direction would be to use the LFA framework in similar ways as has been done for spatial multigrid, by optimizing algorithmic parameters within relaxation and coarse-grid correction.⁴³

ACKNOWLEDGMENTS

We are very grateful to Irad Yavneh pointing us to his work in Reference 39, and for initially explaining to us the possibility of a connection between MGRIT and classical spatial multigrid methods for advection-dominated problems from the perspective of characteristic components.

References

1. Gander MJ. 50 Years of Time Parallel Time Integration. In: *Contrib. Math. Comput. Sci.* Springer International Publishing; 2015. p. 69–113.
2. Ong BW, and Schroder JB. Applications of time parallelization. *Comput Vis Sci.* 2020;**23**(1).
3. Falgout RD, Friedhoff S, Kolev TV, MacLachlan SP, and Schroder JB. Parallel time integration with multigrid. *SIAM J Sci Comput.* 2014;**14**(1):951–952.
4. Lions JL, Maday Y, and Turinici G. Résolution d’EDP par un schéma en temps pararéel. *CR Acad Sci-Series I-Mathematics.* 2001;**332**(7):661–668.
5. Chen F, Hesthaven JS, and Zhu X. On the use of reduced basis methods to accelerate and stabilize the Parareal method. In: *Reduced Order Methods for modeling and computational reduction.* Springer; 2014. p. 187–214.
6. Dai X, and Maday Y. Stable Parareal in time method for first-and second-order hyperbolic systems. *SIAM J Sci Comput.* 2013;**35**(1):A52–A78.
7. De Sterck H, Falgout RD, Friedhoff S, Krzysik OA, and MacLachlan SP. Optimizing multigrid reduction-in-time and Parareal coarse-grid operators for linear advection. *Numer Linear Algebra Appl.* 2021;**28**(4).
8. Dobrev VA, Kolev T, Petersson NA, and Schroder JB. Two-Level Convergence Theory for Multigrid Reduction in Time (MGRIT). *SIAM J Sci Comput.* 2017;**39**(5):S501–S527.
9. Gander MJ, and Vandewalle S. Analysis of the Parareal time-parallel time-integration method. *SIAM J Sci Comput.* 2007;**29**(2):556–578.
10. Gander MJ. Analysis of the Parareal algorithm applied to hyperbolic problems using characteristics. *Soc Esp Mat Apl.* 2008;**42**:21–35.
11. Gander MJ, and Lunet T. Toward error estimates for general space-time discretizations of the advection equation. *Comput Vis Sci.* 2020;**23**(1-4).
12. Hessesenthaler A, Nordsletten D, Röhrle O, Schroder JB, and Falgout RD. Convergence of the multigrid reduction in time algorithm for the linear elasticity equations. *Numer Linear Algebra Appl.* 2018;**25**(3):e2155.
13. Howse AJM, De Sterck H, Falgout RD, MacLachlan S, and Schroder J. Parallel-in-time multigrid with adaptive spatial coarsening for the linear advection and inviscid Burgers equations. *SIAM J Sci Comput.* 2019;**41**(1):A538–A565.
14. Howse A. *Nonlinear Preconditioning Methods for Optimization and Parallel-In-Time Methods for 1D Scalar Hyperbolic Partial Differential Equations.* University of Waterloo. Waterloo, Canada; 2017.
15. Krzysik OA. *Multilevel parallel-in-time methods for advection-dominated PDEs.* Monash University. 2021;.
16. Nielsen AS, Brunner G, and Hesthaven JS. Communication-aware adaptive Parareal with application to a nonlinear hyperbolic system of partial differential equations. *J Comput Phys.* 2018;**371**:483–505.
17. Ruprecht D, and Krause R. Explicit parallel-in-time integration of a linear acoustic-advection system. *Comput & Fluids.* 2012;**59**:72–83.
18. Ruprecht D. Wave propagation characteristics of Parareal. *Comput Vis Sci.* 2018;**19**(1-2):1–17.
19. Schmitt A, Schreiber M, Peixoto P, and Schäfer M. A numerical study of a semi-Lagrangian Parareal method applied to the viscous Burgers equation. *Comput Vis Sci.* 2018;**19**(1-2):45–57.
20. Schroder JB. On the Use of Artificial Dissipation for Hyperbolic Problems and Multigrid Reduction in Time (MGRIT); 2018. LLNL Tech Report LLNL-TR-750825.

21. Steiner J, Ruprecht D, Speck R, and Krause R. Convergence of Parareal for the Navier-Stokes equations depending on the Reynolds number. In: Numerical Mathematics and Advanced Applications-ENUMATH 2013. Springer; 2015. p. 195–202.
22. McDonald E, Pestana J, and Wathen A. Preconditioning and Iterative Solution of All-at-Once Systems for Evolutionary Partial Differential Equations. *SIAM J Sci Comput.* 2018;**40**(2):A1012–A1033.
23. Gander MJ, Halpern L, Rannou J, and Ryan J. A Direct Time Parallel Solver by Diagonalization for the Wave Equation. *SIAM J Sci Comput.* 2019;**41**(1):A220–A245.
24. Gander MJ, and Wu SL. A Diagonalization-Based Parareal Algorithm for Dissipative and Wave Propagation Problems. *SIAM J Numer Anal.* 2020;**58**(5):2981–3009.
25. Liu J, and Wu SL. A fast block α -circulant preconditioner for all-at-once systems from wave equations. *SIAM J Matrix Anal Appl.* 2020;**41**(4):1912–1943.
26. Liu J, Wang XS, Wu SL, and Zhou T. A well-conditioned direct PinT algorithm for first- and second-order evolutionary equations. *Adv Comput Math.* 2022;**48**(3).
27. Maday Y, and Rønquist EM. Parallelization in time through tensor-product space–time solvers. *C R Acad Sci Paris.* 2008;**346**(1-2):113–118.
28. De Sterck H, Friedhoff S, Howse AJM, and MacLachlan SP. Convergence analysis for parallel-in-time solution of hyperbolic systems. *Numer Linear Algebra Appl.* 2020;**27**(1):e2271.
29. Friedhoff S, and MacLachlan S. A generalized predictive analysis tool for multigrid methods. *Numer Linear Alg Appl.* 2015;**22**:618–647.
30. Gander MJ, Kwok F, and Zhang H. Multigrid interpretations of the Parareal algorithm leading to an overlapping variant and MGRIT. *Comput Vis Sci.* 2018;**19**(3-4):59–74.
31. Henthenthaler A, Southworth BS, Nordsletten D, Röhrle O, Falgout RD, and Schroder JB. Multilevel convergence analysis of multigrid-reduction-in-time. *SIAM J Sci Comput.* 2020;**42**(2):A771–A796.
32. Southworth BS. Necessary conditions and tight two-level convergence bounds for Parareal and multigrid reduction in time. *SIAM J Matrix Anal Appl.* 2019;**40**(2):564–608.
33. Brandt A. Multi-level adaptive solutions to boundary-value problems. *Math Comp.* 1977;**31**(138):333–333.
34. Brandt A. Multigrid Solvers for Non-Elliptic and Singular-Perturbation Steady-State Problems; 1981. The Weizmann Institute of Science, Rehovot, Israel. (unpublished).
35. Stüben K, and Trottenberg U. Multigrid methods: Fundamental algorithms, model problem analysis and applications. In: Lecture Notes in Mathematics. Springer Berlin Heidelberg; 1982. p. 1–176.
36. Vandewalle S, and Horton G. Fourier mode analysis of the multigrid waveform relaxation and time-parallel multigrid methods. *Computing.* 1995;**54**(4):317–330.
37. Trottenberg U, Oosterlee CW, and Schuller A. Multigrid. Academic press; 2001.
38. Wienands RR, and Joppich WW. Practical Fourier analysis for multigrid methods. Boca Raton, FL: Chapman & Hall/CRC; 2005.
39. Yavneh I. Coarse-Grid Correction for Nonelliptic and Singular Perturbation Problems. *SIAM J Sci Comput.* 1998;**19**(5):1682–1699.
40. Friedhoff S, MacLachlan S, and Börgers C. Local Fourier Analysis of Space-Time Relaxation and Multigrid Schemes. *SIAM J Sci Comput.* 2013;**35**(5):S250–S276.
41. Gander MJ, Jiang YL, Song B, and Zhang H. Analysis of Two Parareal Algorithms for Time-Periodic Problems. *SIAM J Sci Comput.* 2013;**35**(5):A2393–A2415.

42. Gander MJ, and Neumuller M. Analysis of a new space-time parallel multigrid algorithm for parabolic problems. *SIAM J Sci Comput.* 2016;**38**(4):A2173–A2208.
43. Brown J, He Y, MacLachlan S, Menickelly M, and Wild SM. Tuning multigrid methods with robust optimization and local Fourier analysis. *SIAM J Sci Comput.* 2021;**43**(1):A109–A138.
44. Southworth BS, Mitchell W, Hessenthaler A, and Danieli F. Tight Two-Level Convergence of Linear Parareal and MGRIT: Extensions and Implications in Practice. In: *Parallel-in-Time Integration Methods*. Springer International Publishing; 2021. p. 1–31.
45. Brandt A, and Yavneh I. Accelerated Multigrid Convergence and High-Reynolds Recirculating Flows. *SIAM J Sci Comput.* 1993;**14**(3):607–626.
46. Oosterlee CW, and Washio T. Krylov Subspace Acceleration of Nonlinear Multigrid with Application to Recirculating Flows. *SIAM J Sci Comput.* 2000;**21**(5):1670–1690.
47. Wan WL, and Chan TF. A phase error analysis of multigrid methods for hyperbolic equations. *SIAM J Sci Comput.* 2003;**25**(3):857–880.
48. Bank RE, Wan JWL, and Qu Z. Kernel Preserving Multigrid Methods for Convection-Diffusion Equations. *SIAM J Matrix Anal Appl.* 2006;**27**(4):1150–1171.
49. Yavneh I, and Weinzierl M. Nonsymmetric Black Box multigrid with coarsening by three. *Numerical Linear Algebra with Applications.* 2012;**19**(2):194–209.
50. De Sterck H, Falgout RD, and Krzysik OA. Fast multigrid reduction-in-time for advection via modified semi-Lagrangian coarse-grid operators. *SIAM J Sci Comput.* 2023;**45**(4):A1890–A1916.
51. De Sterck H, Falgout RD, Krzysik OA, and Schroder JB. Efficient multigrid reduction-in-time for method-of-lines discretizations of linear advection. *J Sci Comput.* 2023;**96**(1).
52. De Sterck H, Falgout RD, Krzysik OA, and Schroder JB. Parallel-in-time solution of one-dimensional, scalar, nonlinear conservation laws;. In preparation.
53. Hessenthaler A, Falgout RD, Schroder JB, de Vecchi A, Nordsletten D, and Röhrle O. Time-periodic steady-state solution of fluid-structure interaction and cardiac flow problems through multigrid-reduction-in-time. *Comput Methods Appl Mech Engrg.* 2022;**389**:114368.
54. Durrant DR. *Numerical Methods for Fluid Dynamics*. 2nd ed. Springer New York; 2010.
55. Falcone M, and Ferretti R. *Semi-Lagrangian Approximation Schemes for Linear and Hamilton Jacobi Equations*. CAMBRIDGE; 2014.
56. Brandt A, and Yavneh I. On multigrid solution of high-reynolds incompressible entering flows. *J Comput Phys.* 1992;**101**(1):151–164.
57. Yavneh I, Venner CH, and Brandt A. Fast Multigrid Solution of the Advection Problem with Closed Characteristics. *SIAM J Sci Comput.* 1998;**19**(1):111–125.
58. Danieli F, and MacLachlan S. Multigrid reduction in time for non-linear hyperbolic equations. *Electron Trans Numer Anal.* 2023;**58**:43–65.
59. Vargas DA, Falgout RD, Günther S, and Schroder JB. Multigrid reduction in time for chaotic dynamical systems. *SIAM J Sci Comput.* 2023;**45**(4):A2019–A2042.



APPENDIX

A ERROR PROPAGATION OF THE CONSTANT MODE

Lemma 4. Suppose there exists an index $i_* \in \{1, \dots, n_x\}$ such that $\lambda_{i_*} = \mu_{i_*} = 1$. Then, the associated error propagator (9) is

$$\mathcal{E}_{i_*} = 0. \quad (\text{A1})$$

Proof. Observe that the error propagator \mathcal{E}_{i_*} in (9) corresponds to a scalar initial-value problem with fine-grid time-stepping operator $\lambda_{i_*} = 1$, and coarse-grid time-stepping operator $\mu_{i_*} = 1$ (see, e.g., the expressions for $A_{0,i}$ and $A_{1,i}$ in (10) and (11)). Notice that $\mu_{i_*} = 1 = (\lambda_{i_*})^m$, and therefore that the problem uses an ideal coarse-grid operator. The result (A1) follows immediately by recalling that MGRIT converges to the exact solution in a single iteration when using the ideal coarse-grid operator. \square

B INTERPOLATION MATRICES AND ERROR PROPAGATORS OF RELAXATION

The purpose of this section is to derive convenient representations for the interpolation and relaxation components of the MGRIT error propagator \mathcal{E} in (7).

To begin, it is useful to define a CF-interval as a C-point and the $m-1$ F-points that follow it. We denote the k th such CF-block of a space-time vector $\mathbf{u} = (\mathbf{u}_0, \mathbf{u}_1, \dots, \mathbf{u}_{n_t-1})^\top \in \mathbb{R}^{n_t n_x}$ by

$$\hat{\mathbf{u}}_k = (\mathbf{u}_{km}, \mathbf{u}_{km+1}, \dots, \mathbf{u}_{km+m-1})^\top \in \mathbb{R}^{mn_x}, \quad k \in \{0, \dots, n_t/m-1\}. \quad (\text{B2})$$

Furthermore, the j th vector in the k th CF-block is denoted as $\hat{\mathbf{u}}_{k,j} = \mathbf{u}_{km+j}$, $j \in \{0, \dots, m-1\}$.

We now consider the interpolation operator. Recall that the interpolation operator P in (7) is based on injection. That is, P maps the k th C-point variable $\mathbf{u}_{km} \in \mathbb{R}^{n_x}$ as

$$\mathbf{u}_{km} \mapsto \begin{bmatrix} \mathbf{u}_{km} \\ \mathbf{0} \\ \vdots \\ \mathbf{0} \end{bmatrix} = (\mathbf{e}_1 \otimes I_{n_x}) \mathbf{u}_{km} \in \mathbb{R}^{mn_x}, \quad (\text{B3})$$

in which $\mathbf{e}_1 \in \mathbb{R}^m$ is the canonical (column-oriented) basis vector in the first direction, and is unrelated to the algebraic error $\mathbf{e}^{(p)}$. Therefore, the global space-time interpolation operator that acts on all n_t/m C-point variables simultaneously is the block diagonal matrix

$$P = I_{n_t/m} \otimes (\mathbf{e}_1 \otimes I_{n_x}). \quad (\text{B4})$$

Note that the transpose of injection, which acts as the restriction operator in (7), is simply

$$P^\top = I_{n_t/m} \otimes (\mathbf{e}_1^\top \otimes I_{n_x}). \quad (\text{B5})$$

Next we consider the more complicated cases of the iteration operators for F- and C-relaxation in (7). To this end, suppose we have some approximation to the true solution of the system $A_0 \mathbf{u} = \mathbf{b}$ denoted by $\mathbf{w}^{(0)} \approx \mathbf{u}$. Then, as described in Section 2.1, F-relaxation generates a new approximation $\mathbf{w}^{(0)} \mapsto \mathbf{w}^{(1)}$ such that C-point values of $\mathbf{w}^{(1)}$ are unchanged from those of $\mathbf{w}^{(0)}$, and F-point values of $\mathbf{w}^{(1)}$ have zero residual. In other words, F-relaxation represents an exact solve for the F-point variables of the system $A_0 \mathbf{w}^{(1)} = \mathbf{b}$, where C-point variables in $\mathbf{w}^{(1)}$ are equal to those in $\mathbf{w}^{(0)}$. Therefore, on the k th CF-block, $k \in \{0, 1, \dots, n_t/m-1\}$, F-relaxation can be expressed as the update

$$\begin{aligned} \hat{\mathbf{w}}_{k,0}^{(1)} &= \hat{\mathbf{w}}_{k,0}^{(0)}, \\ \hat{\mathbf{w}}_{k,j}^{(1)} &= \Phi^j \hat{\mathbf{w}}_{k,0}^{(0)} + \hat{\mathbf{b}}_{k,j}, \quad j \in \{1, \dots, m-1\}. \end{aligned} \quad (\text{B6})$$

Replacing the approximations $\mathbf{w}^{(q)}$ via the error equations $\mathbf{w}^{(q)} = \mathbf{u} - \mathbf{e}^{(q)}$ leads to

$$\begin{aligned} \hat{\mathbf{u}}_{k,0} - \hat{\mathbf{e}}_{k,0}^{(1)} &= \hat{\mathbf{u}}_{k,0} - \hat{\mathbf{e}}_{k,0}^{(0)}, \\ \hat{\mathbf{u}}_{k,j} - \hat{\mathbf{e}}_{k,j}^{(1)} &= \Phi^j (\hat{\mathbf{u}}_{k,0} - \hat{\mathbf{e}}_{k,0}^{(0)}) + \hat{\mathbf{b}}_{k,j} = (\Phi^j \hat{\mathbf{u}}_{k,0} + \hat{\mathbf{b}}_{k,j}) - \Phi^j \hat{\mathbf{e}}_{k,0}^{(0)}, \end{aligned} \quad (\text{B7})$$

for $j \in \{1, \dots, m-1\}$, with the last equality following from the linearity of Φ . Note that the exact solution \mathbf{u} is a fixed-point of the update (B6), $\hat{\mathbf{u}}_{k,j} = \Phi^j \hat{\mathbf{u}}_{k,0} + \hat{\mathbf{b}}_{k,j}$, $j \in \{1, \dots, m-1\}$. Therefore, update (B7) can be recast in terms of the error as

$$\begin{aligned}\hat{\mathbf{e}}_{k,0}^{(1)} &= \hat{\mathbf{e}}_{k,0}^{(0)}, \\ \hat{\mathbf{e}}_{k,j}^{(1)} &= \Phi^j \hat{\mathbf{e}}_{k,0}^{(0)}, \quad j \in \{1, \dots, m-1\}.\end{aligned}\tag{B8}$$

Expressed in CF-block form, update (B8) is

$$\hat{\mathbf{e}}_k^{(1)} = \begin{bmatrix} I & 0 & \dots & 0 \\ \Phi & 0 & \dots & 0 \\ \vdots & \vdots & \dots & \vdots \\ \Phi^{m-1} & 0 & \dots & 0 \end{bmatrix} \hat{\mathbf{e}}_k^{(0)} = [e_1^\top \otimes v(\Phi)] \hat{\mathbf{e}}_k^{(0)},\tag{B9}$$

with the function v defined in (5). Thus, based on (B9), the error propagator for F-relaxation that acts on all CF-blocks $k = 0, \dots, n_t/m - 1$ simultaneously is the block diagonal matrix

$$S^F = I_{n_t/m} \otimes [e_1^\top \otimes v(\Phi)].\tag{B10}$$

Now consider C-relaxation. Recall from Section 2.1 that C-relaxation leaves F-point values unchanged and updates C-points such that they have zero residuals. In other words, C-relaxation represents an exact solve for the C-point variables of the system $A_0 \mathbf{w}^{(1)} = \mathbf{b}$, where F-point variables in $\mathbf{w}^{(1)}$ are equal to those in $\mathbf{w}^{(0)}$. Therefore, the C-point update on variables in the k th CF-interval, $k \in \{1, \dots, n_t/m - 1\}$, may be written

$$\begin{aligned}\hat{\mathbf{w}}_{k,0}^{(1)} &= \Phi \hat{\mathbf{w}}_{k-1,m-1}^{(0)} + \hat{\mathbf{b}}_{k,0}, \\ \hat{\mathbf{w}}_{k,j}^{(1)} &= \hat{\mathbf{w}}_{k,j}^{(0)}, \quad j \in \{1, \dots, m-1\}.\end{aligned}\tag{B11}$$

Using the same logic as for F-relaxation above, (B11) can be rewritten as the following update on the error,

$$\hat{\mathbf{e}}_k^{(1)} = \begin{bmatrix} 0 & 0 & \dots & \Phi \\ 0 & 0 & \dots & 0 \\ \vdots & \vdots & \dots & \vdots \\ 0 & 0 & \dots & 0 \end{bmatrix} \hat{\mathbf{e}}_{k-1}^{(0)} + \begin{bmatrix} 0 & & & \\ & I_n & & \\ & & \ddots & \\ & & & I_n \end{bmatrix} \hat{\mathbf{e}}_k^{(0)}.\tag{B12}$$

Recall that in our formulation of \mathcal{E} given by (7), a C-relaxation is always followed by an F-relaxation to create a CF-relaxation. Combining (B9) and (B12), it is easy to show that the error update for a CF-relaxation is simply

$$\hat{\mathbf{e}}_k^{(1)} = \begin{bmatrix} 0 & \dots & 0 & \Phi \\ 0 & \dots & 0 & \Phi^2 \\ \vdots & \dots & \vdots & \vdots \\ 0 & \dots & 0 & \Phi^m \end{bmatrix} \hat{\mathbf{e}}_{k-1}^{(0)} = [e_m^\top \otimes v(\Phi)\Phi] \hat{\mathbf{e}}_{k-1}^{(0)},\tag{B13}$$

Therefore, the error propagator for CF-relaxation that acts on all CF-blocks $k = 0, \dots, n_t/m - 1$ simultaneously is the block lower bidiagonal matrix

$$S^{CF} = L_{n_t/m} \otimes [e_m^\top \otimes v(\Phi)\Phi].\tag{B14}$$

C DERIVATIONS OF FOURIER SYMBOLS

C.1 Proof of Lemma 1 (Fourier symbol of F-relaxation)

Proof. From the representation of $\hat{S}_i^F(\theta)$ given by (35), its (p, q) th element is

$$\left[\hat{S}_i^F(\theta) \right]_{p,q} = \left\langle \boldsymbol{\varphi}_0\left(\theta + \frac{2\pi p}{m}\right), S_i^F \boldsymbol{\varphi}_0\left(\theta + \frac{2\pi q}{m}\right) \right\rangle, \quad p, q \in \{0, \dots, m-1\}.\tag{C15}$$

We begin by considering the vector in the right-hand side of this inner product. Using the definition of S_i^F given in (13), the j th element of the vector $S_i^F \boldsymbol{\varphi}_0(\theta + \frac{2\pi q}{m})$ is

$$\left[S_i^F \boldsymbol{\varphi}_0(\theta + \frac{2\pi q}{m}) \right]_j = \lambda_i^{j \bmod m} \exp \left[\frac{j}{\delta t} (\theta + \frac{2\pi q}{m}) (j - j \bmod m) \delta t \right], \quad (C16)$$

$$= \underbrace{\left[\lambda_i \exp \left(-i(\theta + \frac{2\pi q}{m}) \right) \right]^{j \bmod m}}_{=: \zeta_i(\theta, q)} \left[\boldsymbol{\varphi}_0(\theta + \frac{2\pi q}{m}) \right]_j. \quad (C17)$$

Now, considering the inner product (C15) and the definition of $\zeta_i(\theta, q)$ in (C17), some algebra gives

$$\left[\hat{S}_i^F(\theta) \right]_{p,q} = \lim_{n_i \rightarrow \infty} \frac{1}{n_i} \sum_{k=0}^{n_i-1} [\zeta_i(\theta, q)]^{k \bmod m} \exp \left[\frac{-i}{\delta t} (\theta + \frac{2\pi p}{m}) k \delta t \right] \exp \left[\frac{j}{\delta t} (\theta + \frac{2\pi q}{m}) k \delta t \right], \quad (C18)$$

$$= \lim_{n_i \rightarrow \infty} \frac{1}{n_i} \sum_{k=0}^{n_i-1} [\zeta_i(\theta, q)]^{k \bmod m} \exp \left(\frac{2\pi i k}{m} (q - p) \right), \quad (C19)$$

$$= \lim_{n_i \rightarrow \infty} \frac{1}{n_i} \sum_{r=0}^{m-1} \left([\zeta_i(\theta, q)]^r \left[\sum_{k=0}^{\frac{n_i}{m}-1} \exp \left(\frac{2\pi i (km+r)}{m} (q - p) \right) \right] \right), \quad (C20)$$

$$= \lim_{n_i \rightarrow \infty} \frac{1}{n_i} \sum_{r=0}^{m-1} \left([\zeta_i(\theta, q)]^r \left[\exp \left(\frac{2\pi i r}{m} (q - p) \right) \sum_{k=0}^{\frac{n_i}{m}-1} \exp \left(2\pi i k (q - p) \right) \right] \right), \quad (C21)$$

$$= \lim_{n_i \rightarrow \infty} \frac{1}{n_i} \sum_{r=0}^{m-1} \left([\zeta_i(\theta, q)]^r \left[\frac{n_i}{m} \exp \left(\frac{2\pi i r}{m} (q - p) \right) \right] \right), \quad (C22)$$

$$= \frac{1}{m} \sum_{r=0}^{m-1} \left[\zeta_i(\theta, q) \exp \left(\frac{2\pi i}{m} (q - p) \right) \right]^r, \quad (C23)$$

Substituting $\zeta_i(\theta, q)$ from (C17) into (C23) and simplifying the geometric sum gives

$$\left[\hat{S}_i^F(\theta) \right]_{p,q} = \frac{1}{m} \sum_{r=0}^{m-1} \left[\lambda_i \exp \left(-i(\theta + \frac{2\pi p}{m}) \right) \right]^r = \frac{1}{m} \frac{1 - (\lambda_i e^{-i\theta})^m}{1 - \exp \left(-i(\theta + \frac{2\pi p}{m}) \right)}. \quad (C24)$$

Observe from (C24) that $\left[\hat{S}_i^F(\theta) \right]_{p,q}$ does not depend on the column index q , but only the row index p . This means that $\hat{S}_i^F(\theta)$ can be expressed as an outer product of the form $\hat{S}_i^F(\theta) = \frac{1}{m} [1 - (\lambda_i e^{-i\theta})^m] \mathbf{a} \mathbf{1}^\top$, for some vector \mathbf{a} whose p th element is $1/[1 - \exp(-i(\theta + \frac{2\pi p}{m}))] = 1/\tilde{A}_{0,i}(\theta + \frac{2\pi p}{m})$, where $\tilde{A}_{0,i}(\theta)$ is the Fourier symbol of $A_{0,i}$ given in (38). Therefore, $\mathbf{a} = [\hat{A}_{0,i}(\theta)]^{-1} \mathbf{1}$, in which $\hat{A}_{0,i}(\theta)$ is the diagonal matrix in (37) holding the Fourier symbols of the harmonics. This gives the result (40) for $\hat{S}_i^F(\theta)$. \square

C.2 Proof of Corollary 1 (Idempotence of F-relaxation)

Proof. Consider first the eigenvalue claims. Since $\hat{S}_i^F(\theta) \in \mathbb{C}^{m \times m}$ has a rank of one (see (40)), it has $m - 1$ zero eigenvalues, and if it is idempotent then its one remaining eigenvalue must be one.

Using the expression for $\hat{S}_i^F(\theta)$ given by (40), its square is

$$\hat{S}_i^F(\theta) \hat{S}_i^F(\theta) = \left(c(\theta) [\hat{A}_{0,i}(\theta)]^{-1} \mathbf{1} \mathbf{1}^\top \right) \left(c(\theta) [\hat{A}_{0,i}(\theta)]^{-1} \mathbf{1} \mathbf{1}^\top \right), \quad (C25)$$

$$= c(\theta) [\hat{A}_{0,i}(\theta)]^{-1} \mathbf{1} \left(\mathbf{1}^\top c(\theta) [\hat{A}_{0,i}(\theta)]^{-1} \mathbf{1} \right) \mathbf{1}^\top, \quad (C26)$$

$$= \left(\mathbf{1}^\top c(\theta) [\hat{A}_{0,i}(\theta)]^{-1} \mathbf{1} \right) \hat{S}_i^F(\theta). \quad (C27)$$

We now show that the inner product in (C27) is one, and, thus, that $\hat{S}_i^F(\theta)$ is idempotent. From Equation (C24) in the proof of Lemma 1, the column vector $c(\theta)[\hat{A}_{0,i}(\theta)]^{-1}\mathbf{1}$ can be written as

$$\left[c(\theta)[\hat{A}_{0,i}(\theta)]^{-1}\mathbf{1} \right]_p = \frac{1}{m} \sum_{r=0}^{m-1} \left[\lambda_i \exp \left(-i \left(\theta + \frac{2\pi p}{m} \right) \right) \right]^r. \quad (\text{C28})$$

Thus, with (C28), the inner product in (C27) can be written as

$$\mathbf{1}^\top c(\theta)[\hat{A}_{0,i}(\theta)]^{-1}\mathbf{1} = \frac{1}{m} \sum_{p=0}^{m-1} \left(\sum_{r=0}^{m-1} \left[\lambda_i \exp \left(-i \left(\theta + \frac{2\pi p}{m} \right) \right) \right]^r \right), \quad (\text{C29})$$

$$= \frac{1}{m} \sum_{r=0}^{m-1} \left[\lambda_i e^{-i\theta} \right]^r \sum_{p=0}^{m-1} \left[\exp \left(\frac{-2\pi i r}{m} \right) \right]^p, \quad (\text{C30})$$

$$= \frac{1}{m} \sum_{r=0}^{m-1} \left[\lambda_i e^{-i\theta} \right]^r m \delta_{r,0}, \quad (\text{C31})$$

$$= 1. \quad (\text{C32})$$

In (C31), $\delta_{r,0}$ denotes the Kronecker delta function, and it has arisen from simplifying the geometric sum over p in the previous equation. \square

C.3 Proof of Lemma 2 (Fourier symbol of pre-relaxation)

Proof. We begin by computing the Fourier symbol for CF-relaxation. From (36), the (p, q) th element of $\hat{S}_i^{\text{CF}}(\theta)$ is equal to

$$\left[\hat{S}_i^{\text{CF}}(\theta) \right]_{p,q} = \left\langle \boldsymbol{\varphi}_0 \left(\theta + \frac{2\pi p}{m} \right), S_i^{\text{CF}} \boldsymbol{\varphi}_0 \left(\theta + \frac{2\pi q}{m} \right) \right\rangle, \quad p, q \in \{0, \dots, m-1\}. \quad (\text{C33})$$

Using the expression for S_i^{CF} given in (14), the j th element of the vector $S_i^{\text{CF}} \boldsymbol{\varphi}_0 \left(\theta + \frac{2\pi q}{m} \right)$ can be written as

$$\left[S_i^{\text{CF}} \boldsymbol{\varphi}_0 \left(\theta + \frac{2\pi q}{m} \right) \right]_j = \lambda_i \lambda_i^{j \bmod m} \exp \left[\frac{i}{\delta t} \left(\theta + \frac{2\pi q}{m} \right) (j-1-j \bmod m) \delta t \right], \quad (\text{C34})$$

$$= \zeta_i(\theta, q) [\zeta_i(\theta, q)]^{j \bmod m} \left[\boldsymbol{\varphi}_0 \left(\theta + \frac{2\pi q}{m} \right) \right]_j, \quad (\text{C35})$$

$$= \zeta_i(\theta, q) \left[S_i^{\text{F}} \boldsymbol{\varphi}_0 \left(\theta + \frac{2\pi q}{m} \right) \right]_j, \quad (\text{C36})$$

where the function $\zeta_i(\theta, q)$ is as in (C17), and $[\zeta_i(\theta, q)]^{j \bmod m} [\boldsymbol{\varphi}_0 \left(\theta + \frac{2\pi q}{m} \right)]_j$ has been replaced with $\left[S_i^{\text{F}} \boldsymbol{\varphi}_0 \left(\theta + \frac{2\pi q}{m} \right) \right]_j$ by using (C17).

Therefore, from (C33) and (C36), the following simple relationship holds between the (p, q) th element of the Fourier symbols of CF- and F-relaxation:

$$\left[\hat{S}_i^{\text{CF}}(\theta) \right]_{p,q} = \zeta_i(\theta, q) \left[\hat{S}_i^{\text{F}}(\theta) \right]_{p,q}. \quad (\text{C37})$$

From its definition (see (C17)), $\zeta_i(\theta, q) = 1 - \tilde{A}_{0,i} \left(\theta + \frac{2\pi q}{m} \right)$, where $\tilde{A}_{0,i}(\theta)$ defined in (38) is the Fourier symbol of $A_{0,i}$. Thus, from (C37) and (40), the Fourier symbol of CF-relaxation may be expressed as

$$\hat{S}_i^{\text{CF}}(\theta) = \hat{S}_i^{\text{F}}(\theta) \left[I - \hat{A}_{0,i}(\theta) \right] = c(\theta) [\hat{A}_{0,i}(\theta)]^{-1} \mathbf{1}^\top \left[I - \hat{A}_{0,i}(\theta) \right], \quad (\text{C38})$$

in which $\hat{A}_{0,i}(\theta)$ is the diagonal matrix holding the Fourier symbols of the harmonics (see (37)). This proves (42), the first claim of the lemma.

Now we consider taking powers of the Fourier symbol. Exploiting the rank-1 structure of $\hat{S}_i^{\text{CF}}(\theta)$ in (C38), any power $v \in \mathbb{N}$ of the matrix can be computed as

$$\left[\hat{S}_i^{\text{CF}}(\theta) \right]^v = \left(c(\theta) [\hat{A}_{0,i}(\theta)]^{-1} \mathbf{1}^\top \left[I - \hat{A}_{0,i}(\theta) \right] \right)^v, \quad (\text{C39})$$

$$= c(\theta) [\hat{A}_{0,i}(\theta)]^{-1} \mathbf{1} \left(\mathbf{1}^\top \left[I - \hat{A}_{0,i}(\theta) \right] c(\theta) [\hat{A}_{0,i}(\theta)]^{-1} \mathbf{1} \right)^{v-1} \mathbf{1}^\top \left[I - \hat{A}_{0,i}(\theta) \right], \quad (\text{C40})$$

$$= \left(\mathbf{1}^\top c(\theta) [\hat{A}_{0,i}(\theta)]^{-1} \mathbf{1} - c(\theta) \mathbf{1}^\top \mathbf{1} \right)^{\nu-1} \hat{S}_i^{\text{CF}}(\theta), \quad \nu \in \mathbb{N}. \quad (\text{C41})$$

The remaining problem is thus one of evaluating the two inner products in (C41): $\mathbf{1}^\top c(\theta) [\hat{A}_{0,i}(\theta)]^{-1} \mathbf{1}$, and $c(\theta) \mathbf{1}^\top \mathbf{1}$. The first inner product was already shown to be one in the proof of Corollary 1 (specifically, see (C32)), and the second is simply $c(\theta) \mathbf{1}^\top \mathbf{1} = mc(\theta)$. Thus, the function raised to the power $\nu - 1$ in (C41) is simply

$$\mathbf{1}^\top c(\theta) [\hat{A}_{0,i}(\theta)]^{-1} \mathbf{1} - c(\theta) \mathbf{1}^\top \mathbf{1} = 1 - mc(\theta) = (\lambda_i e^{-i\theta})^m. \quad (\text{C42})$$

Substituting this into (C41) leads immediately to

$$[\hat{S}_i^{\text{CF}}(\theta)]^\nu = (\lambda_i e^{-i\theta})^{(\nu-1)m} \hat{S}_i^{\text{CF}}(\theta), \quad \nu \in \mathbb{N}. \quad (\text{C43})$$

Finally, to complete the proof, consider the product of the CF- and F-relaxation Fourier symbols. Using the same rank-1 exploit as above and using (C42) gives

$$\hat{S}_i^{\text{CF}}(\theta) \hat{S}_i^{\text{F}}(\theta) = \left(c(\theta) [\hat{A}_{0,i}(\theta)]^{-1} \mathbf{1} \mathbf{1}^\top \left[I - \hat{A}_{0,i}(\theta) \right] \right) \left(c(\theta) [\hat{A}_{0,i}(\theta)]^{-1} \mathbf{1} \mathbf{1}^\top \right), \quad (\text{C44})$$

$$= c(\theta) [\hat{A}_{0,i}(\theta)]^{-1} \mathbf{1} \left(\mathbf{1}^\top \left[I - \hat{A}_{0,i}(\theta) \right] c(\theta) [\hat{A}_{0,i}(\theta)]^{-1} \mathbf{1} \right) \mathbf{1}^\top, \quad (\text{C45})$$

$$= (\lambda_i e^{-i\theta})^m \hat{S}_i^{\text{F}}(\theta). \quad (\text{C46})$$

Combining this result with (C43) leads immediately to the claimed result of (43) that $[\hat{S}_i^{\text{CF}}(\theta)]^\nu \hat{S}_i^{\text{F}}(\theta) = (\lambda_i e^{-i\theta})^{m\nu} \hat{S}_i^{\text{F}}(\theta)$ for $\nu \in \mathbb{N}_0$. \square

C.4 Proof of Theorem 1 (Error propagator Fourier symbol)

Proof. We begin by forming $\hat{\mathcal{K}}_i(\theta)$ from (31), which is the coarse-grid correction component of $\hat{\mathcal{E}}_i(\theta)$. Using the interpolation Fourier symbol (39), and exploiting that the Fourier symbol of the coarse-grid operator is a scalar (see (37)), we have

$$\hat{\mathcal{K}}_i(\theta) = I_m - \frac{1}{m} [\hat{A}_{1,i}(m\theta)]^{-1} \mathbf{1} \mathbf{1}^\top \hat{A}_{0,i}(\theta). \quad (\text{C47})$$

Substituting this into the expression for $\hat{\mathcal{E}}_i(\theta)$ given in (30), and using the result from (43) that $[\hat{S}_i^{\text{CF}}(\theta)]^\nu \hat{S}_i^{\text{F}}(\theta) = (\lambda_i e^{-i\theta})^{m\nu} \hat{S}_i^{\text{F}}(\theta)$ gives

$$\hat{\mathcal{E}}_i(\theta) = \hat{S}_i^{\text{F}}(\theta) \left(I_m - \frac{1}{m} [\hat{A}_{1,i}(m\theta)]^{-1} \mathbf{1} \mathbf{1}^\top \hat{A}_{0,i}(\theta) \right) [\hat{S}_i^{\text{CF}}(\theta)]^\nu \hat{S}_i^{\text{F}}(\theta), \quad (\text{C48})$$

$$= (\lambda_i e^{-i\theta})^{m\nu} \left([\hat{S}_i^{\text{F}}(\theta)]^2 - \frac{1}{m} [\hat{A}_{1,i}(m\theta)]^{-1} [\hat{S}_i^{\text{F}}(\theta) \mathbf{1} \mathbf{1}^\top \hat{A}_{0,i}(\theta) \hat{S}_i^{\text{F}}(\theta)] \right). \quad (\text{C49})$$

From (40), recall that $\hat{S}_i^{\text{F}}(\theta) = c(\theta) [\hat{A}_{0,i}(\theta)]^{-1} \mathbf{1} \mathbf{1}^\top$, with c a scalar. Using this, and that $\mathbf{1}^\top \mathbf{1} = m$, the last term in closed parentheses in (C49) can be rewritten as

$$\hat{S}_i^{\text{F}}(\theta) \left(\mathbf{1} \mathbf{1}^\top \hat{A}_{0,i}(\theta) \hat{S}_i^{\text{F}}(\theta) \right) = \hat{S}_i^{\text{F}}(\theta) \left(\mathbf{1} \mathbf{1}^\top \hat{A}_{0,i}(\theta) c(\theta) [\hat{A}_{0,i}(\theta)]^{-1} \mathbf{1} \mathbf{1}^\top \right), \quad (\text{C50})$$

$$= \hat{S}_i^{\text{F}}(\theta) \left(c(\theta) \mathbf{1} \mathbf{1}^\top \mathbf{1} \mathbf{1}^\top \right), \quad (\text{C51})$$

$$= c(\theta) c(\theta) [\hat{A}_{0,i}(\theta)]^{-1} \mathbf{1} \mathbf{1}^\top \mathbf{1} \mathbf{1}^\top, \quad (\text{C52})$$

$$= m^2 c(\theta) \hat{S}_i^{\text{F}}(\theta). \quad (\text{C53})$$

Substituting this result into (C49) gives the error propagator Fourier symbol as

$$\hat{\mathcal{E}}_i(\theta) = (\lambda_i e^{-i\theta})^{m\nu} \left([\hat{S}_i^{\text{F}}(\theta)]^2 - mc(\theta) [\hat{A}_{1,i}(m\theta)]^{-1} \hat{S}_i^{\text{F}}(\theta) \right), \quad (\text{C54})$$

$$= (\lambda_i e^{-i\theta})^{m\nu} \left(1 - mc(\theta) [\hat{A}_{1,i}(m\theta)]^{-1} \right) \hat{S}_i^{\text{F}}(\theta), \quad (\text{C55})$$

where the second equality follows by the idempotence of $\hat{S}_i^{\text{F}}(\theta)$ (see Corollary 1), and then pulling out the common factor of $\hat{S}_i^{\text{F}}(\theta)$.

Finally, using the definition of $c(\theta)$ given in (41), and the expression for $\hat{A}_{1,i}(m\theta)$ given by (37), we get

$$1 - mc(\theta) [\hat{A}_{1,i}(m\theta)]^{-1} = \frac{\hat{A}_{1,i}(m\theta) - mc(\theta)}{\hat{A}_{1,i}(m\theta)} = \frac{\lambda_i^m e^{-im\theta} - \mu_i e^{-im\theta}}{1 - \mu_i e^{-im\theta}} = \frac{\lambda_i^m - \mu_i}{e^{im\theta} - \mu_i}. \quad (C56)$$

Substituting this into (C55) yields the claimed form of $\hat{\mathcal{E}}_i(\theta)$ given by (44). \square

D EIGENVALUE ESTIMATES

D.1 Semi-Lagrangian discretizations

In this appendix, we present eigenvalue estimates for the time-stepping operators of semi-Lagrangian discretizations by invoking truncation error estimates from our recent work in Reference 50. To this end, consider the matrix \mathcal{D}_{p+1} from De Sterck et al.⁵⁰

Definition 2. Define the matrix $\mathcal{D}_{p+1} \in \mathbb{R}^{n_x \times n_x}$ such that $h^{-(p+1)} \mathcal{D}_{p+1}$ represents a finite-difference rule for approximating the $p + 1$ st derivative of periodic grid functions. Let $\mathbf{v} = (v(x_1), \dots, v(x_{n_x}))^\top \in \mathbb{R}^{n_x}$ denote a vector of a periodic function $v(x)$ evaluated on the spatial mesh. Then, if the finite-difference rule is of order $s \in \mathbb{N}$ and v is at least $p + 1 + s$ times continuously differentiable

$$\left(\frac{\mathcal{D}_{p+1}}{h^{p+1}} \mathbf{v} \right)_i = \frac{d^{p+1} v}{dx^{p+1}} \Big|_{x_i} + \mathcal{O}(h^s), \quad i \in \{1, \dots, n_x\}. \quad (D57)$$

Since the mesh points are equispaced, the matrix \mathcal{D}_{p+1} is circulant.

Now, consider the following truncation error estimate, which is a simplified version of Lemma 3.1 from De Sterck et al.⁵⁰

Lemma 5 (Truncation error estimate of $\mathcal{S}_p^{(\delta t)}$). Define $\mathbf{u}(t) \in \mathbb{R}^{n_x}$ as the vector composed of the exact solution of the advection equation sampled in space at the mesh points \mathbf{x} and at time t . Suppose that p is odd. Then, the local truncation error of the semi-Lagrangian discretization $\mathcal{S}_p^{(\delta t)}$ can be expressed as

$$\mathbf{u}(t_{n+1}) - \mathcal{S}_p^{(\delta t)} \mathbf{u}(t_n) = h^{p+1} f_{p+1}(\varepsilon^{(\delta t)}) \frac{\mathcal{D}_{p+1}}{h^{p+1}} \mathbf{u}(t_{n+1}) + \mathcal{O}(h^{p+2}), \quad (D58)$$

in which $\varepsilon^{(\delta t)}$ is the mesh-normalized distance from a departure point to its east-neighboring mesh point. The function f_{p+1} in (D58) is the following degree $p + 1$ polynomial

$$f_{p+1}(z) = \frac{1}{(p+1)!} \prod_{q=-\frac{p+1}{2}}^{\frac{p-1}{2}} (q + z). \quad (D59)$$

The result of Lemma 5 is now used to develop an eigenvalue estimate for the semi-Lagrangian discretization.

Theorem 7 (Eigenvalue estimates of $\mathcal{S}_p^{(\delta t)}$ and Ψ_{ideal}). Let $s_p^{(\delta t)}(\omega)$ denote the eigenvalue of the semi-Lagrangian time-stepping operator $\mathcal{S}_p^{(\delta t)}$ associated with the spatial Fourier mode $\chi(\omega)$ from (70). Analogously, let $[s_p^{(\delta t)}(\omega)]^m$ denote the eigenvalue of the associated ideal coarse-grid operator, $\Psi_{\text{ideal}} = \prod_{k=0}^{m-1} \mathcal{S}_p^{(\delta t)}$. Suppose that p is odd. Then, we have the following estimates for eigenvalues associated with asymptotically smooth Fourier modes (i.e., $\omega = \mathcal{O}(h)$)

$$s_p^{(\delta t)}(\omega) = \exp\left(-\frac{i\omega\alpha\delta t}{h}\right) \left[1 - f_{p+1}(\varepsilon^{(\delta t)}) d_{p+1}(\omega) + \mathcal{O}(\omega^{p+2})\right], \quad (D60)$$

$$[s_p^{(\delta t)}(\omega)]^m = \exp\left(-\frac{i\omega\alpha m\delta t}{h}\right) \left[1 - m f_{p+1}(\varepsilon^{(\delta t)}) d_{p+1}(\omega) + \mathcal{O}(\omega^{p+2})\right], \quad (D61)$$

with $d_{p+1}(\omega)$ the eigenvalue of \mathcal{D}_{p+1} (see Lemma 6 for further details).

Proof. Observe the following function is an exact solution of the advection equation $\frac{\partial u}{\partial t} + \alpha \frac{\partial u}{\partial x} = 0$,

$$u(x, t) = \exp\left(\frac{i\omega}{h}(x - \alpha t)\right) = \exp\left(-\frac{i\omega\alpha t}{h}\right) \chi(\omega). \quad (D62)$$

Thus, the vector from Lemma 5 that is an exact PDE solution sampled at the spatial mesh points can be written as $\mathbf{u}(t) = \exp\left(-\frac{i\omega\alpha t}{h}\right) \chi(\omega)$. Substituting this vector into the truncation error estimate (D58) for $\mathcal{S}_p^{(\delta t)}$ gives the following relation for

asymptotically smooth Fourier modes:

$$\exp\left(-\frac{i\omega\alpha(t_n + \delta t)}{h}\right)\chi(\omega) - \exp\left(-\frac{i\omega\alpha t_n}{h}\right)S_p^{(\delta t)}\chi(\omega) = \exp\left(-\frac{i\omega\alpha(t_n + \delta t)}{h}\right)[f_{p+1}(\epsilon^{(\delta t)})D_{p+1} + \mathcal{O}(\omega^{p+2})]\chi(\omega). \quad (\text{D63})$$

Here, we have re-written the $\mathcal{O}(h^{p+2})$ term from (D58) as $\mathcal{O}(\omega^{p+2})\mathbf{u}(t_{n+1})$, since $\mathcal{O}(h^{p+2}) = \mathcal{O}(\omega^{p+2}) = \mathcal{O}(\omega^{p+2})\mathbf{u}(t_{n+1})$. Rearranging this equation for $S_p^{(\delta t)}\chi(\omega)$ gives

$$S_p^{(\delta t)}\chi(\omega) = \exp\left(-\frac{i\omega\alpha\delta t}{h}\right)\left[1 - f_{p+1}(\epsilon^{(\delta t)})D_{p+1} + \mathcal{O}(\omega^{p+2})\right]\chi(\omega). \quad (\text{D64})$$

Applying $D_{p+1}\chi(\omega) = d_{p+1}(\omega)\chi(\omega)$ in (D64) gives the claim (D60).

The eigenvalue estimate (D61) for the associated ideal coarse-grid operator follows by applying $S_p^{(\delta t)}$ to both sides of (D64) a further $m - 1$ times, each time invoking on the right-hand side the eigenvalue estimate for $S_p^{(\delta t)}$, then collecting terms of size $\mathcal{O}(\omega^{p+2})$ together. \square

The following result estimates the eigenvalues of the matrix D_{p+1} given in Definition 2.

Lemma 6 (Eigenvalue estimate of D_{p+1}). Let $d_{p+1}(\omega)$ denote the eigenvalue of D_{p+1} from Definition 2 associated with the spatial Fourier mode $\chi(\omega)$. Suppose that p is odd. Then, we have the following estimate for eigenvalues associated with asymptotically smooth Fourier modes

$$d_{p+1}(\omega) = (i\omega)^{p+1} + \mathcal{O}(\omega^{p+1+s}) = (-1)^{\frac{p+1}{2}}\omega^{p+1}\left[1 + \mathcal{O}(\omega^s)\right], \quad (\text{D65})$$

with s the order of approximation of D_{p+1} .

Proof. This follows by taking \mathbf{v} in (D57) as the spatial Fourier mode $\chi(\omega)$ from (70), then using that $\omega = \mathcal{O}(h)$ for asymptotically smooth modes. \square

D.2 Modified semi-Lagrangian discretization

Lemma 7. Suppose that p is odd. Consider the modified semi-Lagrangian coarse-grid operator from (3.20) of De Sterck et al.,⁵⁰ $\Psi = \left(I - [f_{p+1}(\epsilon^{(m\delta t)}) - mf_{p+1}(\epsilon^{(\delta t)})]D_{p+1}\right)^{-1}S_p^{(m\delta t)}$. Let $\psi(\omega)$ denote the eigenvalue of Ψ associated with spatial Fourier mode $\chi(\omega)$ from (70). Then, we have the following estimate for eigenvalues of Ψ associated with asymptotically smooth Fourier modes (i.e., $\omega = \mathcal{O}(h)$)

$$\psi(\omega) = \exp\left(-\frac{i\omega\alpha m\delta t}{h}\right)\left(1 - mf_{p+1}(\epsilon^{(\delta t)})d_{p+1}(\omega) + \mathcal{O}(\omega^{p+2})\right), \quad (\text{D66})$$

with $d_{p+1}(\omega)$ the eigenvalue of D_{p+1} (see Lemma 6 for further details).

Proof. Applying Ψ to an asymptotically smooth Fourier mode and then invoking the geometric expansion $\frac{1}{1-\epsilon} = 1 + \epsilon + \mathcal{O}(\epsilon^2)$ gives

$$\Psi\chi(\omega) = \frac{S_p^{(m\delta t)}}{1 - [f_{p+1}(\epsilon^{(m\delta t)}) - mf_{p+1}(\epsilon^{(\delta t)})]d_{p+1}(\omega)}\chi(\omega), \quad (\text{D67})$$

$$= \left(1 + [f_{p+1}(\epsilon^{(m\delta t)}) - mf_{p+1}(\epsilon^{(\delta t)})]d_{p+1}(\omega) + \mathcal{O}([d_{p+1}(\omega)]^2)\right)S_p^{(m\delta t)}\chi(\omega). \quad (\text{D68})$$

The claimed result (D66) follows by substituting into (D68) the estimate for $S_p^{(m\delta t)}$ that arises from (D60), applying the fact that $d_{p+1}(\omega) = \mathcal{O}(\omega^{p+1})$ from (D65), and then collecting together terms of size $\mathcal{O}(\omega^{p+2})$. \square

E REMAINDER OF THE PROOF OF Theorem 5 (CONVERGENCE FACTOR LOWER BOUND)

Here, we continue with the proof of Theorem 5, showing that $\check{\rho}_p(\epsilon^{(\delta t)}) > 1$ when $\epsilon^{(\delta t)} \in \Upsilon_m \cap \left(\frac{2}{3m}, 1 - \frac{2}{3m}\right)$.

Proof. For notational simplicity, write $\epsilon \equiv \epsilon^{(\delta t)}$ throughout the proof. This proof relies on details about $f_{p+1}(\epsilon)$ and $f_{p+1}(m\epsilon - [m\epsilon])$ given in Lems. 4.5 & B.1 of Krzysik,¹⁵ as well as Lemma 8 below. We prove the claim only for the case of $\frac{p+1}{2}$ even corresponding to f_{p+1} being non-negative. The proof extends to $\frac{p+1}{2}$ odd by following through the sign changes on f_{p+1} .

See Figure E1 for examples of the functions $f_{p+1}(\varepsilon)$ and $f_{p+1}(m\varepsilon - \lfloor m\varepsilon \rfloor)$. Specific properties of $f_{p+1}(\varepsilon)$ that we use are that it is symmetric over $\varepsilon \in [0, 1]$, and that it is monotonically increasing on $\varepsilon \in [0, \frac{1}{2}]$ to its only critical point, which is a global maximum at $\varepsilon = \frac{1}{2}$. Additionally, note that $f_{p+1}(m\varepsilon - \lfloor m\varepsilon \rfloor)$ is periodic over $\varepsilon \in [0, 1]$ due to its argument being $\frac{1}{m}$ -periodic in ε . This function has global minima at $\varepsilon = \frac{k}{m}$, $k = 0, \dots, m$ and global maxima at $\varepsilon = \frac{k}{m} + \frac{1}{2m}$, $k = 0, \dots, m-1$, and between these global minima and maxima the function changes monotonically.

Define the function

$$\check{f}(\varepsilon) := mf_{p+1}(\varepsilon) - 2f_{p+1}(m\varepsilon - \lfloor m\varepsilon \rfloor), \quad (\text{E69})$$

motivated by the fact that $\check{f}(\varepsilon) > 1 \iff \check{f}(\varepsilon) > 0$ when $\varepsilon \in \Upsilon_m$. Since $\check{f}(\varepsilon)$ is symmetric on $\varepsilon \in [0, 1]$ we need only consider $\varepsilon \in [0, \frac{1}{2}]$. The proof works by showing that $mf_{p+1}(\varepsilon) > 2f_{p+1}(m\varepsilon - \lfloor m\varepsilon \rfloor)$ for all $\varepsilon \in \mathcal{I} := (\frac{2}{3m}, \frac{1}{2}]$. For $m > 2$ we do this by considering separately the two sub-intervals $\mathcal{I}_1 := (\frac{2}{3m}, \frac{3}{2m}]$ and $\mathcal{I}_2 := [\frac{3}{2m}, \frac{1}{2}]$. The special case of $m = 2$ is described at the end.

Suppose that $m > 2$ and consider $\varepsilon \in \mathcal{I}_2$. From Lemma 8 we have $mf_{p+1}(\varepsilon) > 2f_{p+1}(m\varepsilon - \lfloor m\varepsilon \rfloor)$ at the left-hand boundary of \mathcal{I}_2 , and recall that that $2f_{p+1}(m\varepsilon - \lfloor m\varepsilon \rfloor)$ has a global maximum at this left-hand boundary of \mathcal{I}_2 . Then, since $mf_{p+1}(\varepsilon)$ is monotonically increasing over $\varepsilon \in \mathcal{I}_2$ it follows that $mf_{p+1}(\varepsilon) > 2f_{p+1}(m\varepsilon - \lfloor m\varepsilon \rfloor)$ for all $\varepsilon \in \mathcal{I}_2$.

Suppose that $m > 2$ and consider $\varepsilon \in \mathcal{I}_1$. Recall that $2f_{p+1}(m\varepsilon - \lfloor m\varepsilon \rfloor)$ is monotonically decreasing on a sub-interval of \mathcal{I}_1 given by $\varepsilon \in [\frac{2}{3m}, \frac{1}{m}]$, while it is monotonically increasing on the remainder of \mathcal{I}_1 , $\varepsilon \in [\frac{1}{m}, \frac{3}{2m}]$. Then, since $mf_{p+1}(\varepsilon) > 2f_{p+1}(m\varepsilon - \lfloor m\varepsilon \rfloor)$ at both end points of \mathcal{I}_1 (see Lemma 8), it follows that $mf_{p+1}(\varepsilon) > 2f_{p+1}(m\varepsilon - \lfloor m\varepsilon \rfloor)$ for all $\varepsilon \in \mathcal{I}_1$ because $mf_{p+1}(\varepsilon)$ is monotonically increasing on \mathcal{I}_1 and it is concave up.

Finally, consider the $m = 2$ case. From Lemma 8, we have that $mf_{p+1}(\varepsilon) = 2f_{p+1}(m\varepsilon - \lfloor m\varepsilon \rfloor)$ at $\varepsilon = \frac{2}{3m}$. Then, recall that $mf_{p+1}(\varepsilon)$ is monotonically increasing on $\varepsilon \in [\frac{2}{3m}, \frac{1}{2}]$ and that $2f_{p+1}(m\varepsilon - \lfloor m\varepsilon \rfloor)$ is monotonically decreasing on $\varepsilon \in [\frac{2}{3m}, \frac{1}{2}]$. Therefore, it follows that $mf_{p+1}(\varepsilon) > 2f_{p+1}(m\varepsilon - \lfloor m\varepsilon \rfloor)$ for all $\varepsilon \in (\frac{2}{3m}, \frac{1}{2}]$. \square

Lemma 8. Let $p \in \mathbb{N}$ such that $\frac{p+1}{2}$ is odd, let and $m \in \mathbb{N} \setminus \{1\}$. Let $f_{p+1}(z)$ be the polynomial in (D59). Then,

$$mf_{p+1}(\varepsilon) \geq 2f_{p+1}(m\varepsilon - \lfloor m\varepsilon \rfloor) \quad (\text{E70})$$

holds at $\varepsilon = \frac{3}{2m}$ for $m \geq 3$ without equality (Claim I), and holds at $\varepsilon = \frac{2}{3m}$ with equality for $m = 2$, and without equality for $m \geq 3$ (Claim II).

Proof. It is useful to consider an alternative expression for $f_{p+1}(z)$ than (D59). From (B.8) of Krzysik,¹⁵ for $\frac{p+1}{2}$ even, we have

$$f_{p+1}(z) = \frac{z \left(\frac{p+1}{2} - z \right)}{(p+1)!} \prod_{q=1}^{\frac{p-1}{2}} (q^2 - z^2) \quad (\text{E71})$$

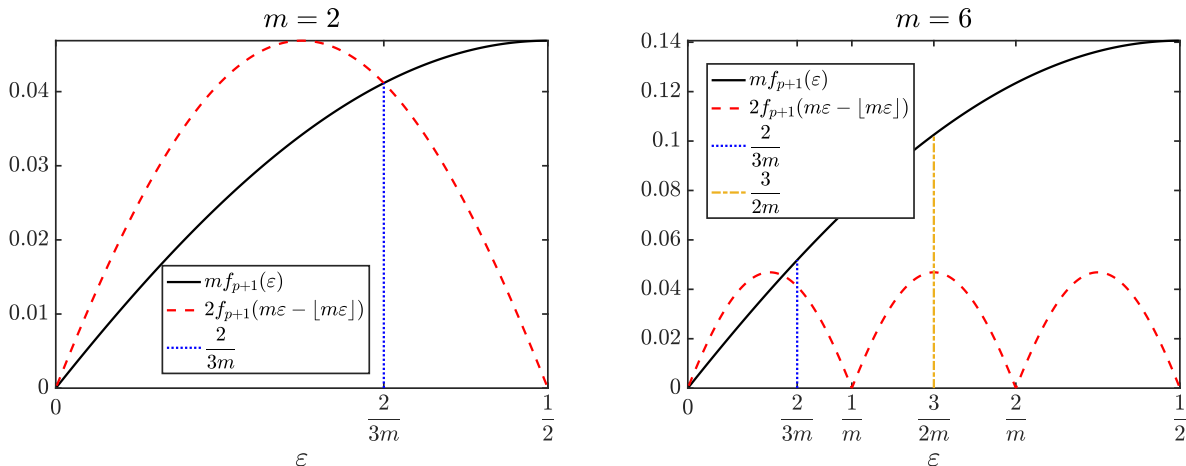


FIGURE E1 Examples of the functions analyzed in Appendix E for $p = 3$, with $m = 2$ (left), and $m = 6$ (right).

Consider Claim I. If $\varepsilon = \frac{3}{2m}$, then $m\varepsilon - \lfloor m\varepsilon \rfloor = \frac{1}{2}$, and (E70) reduces to $mf_{p+1}\left(\frac{3}{2m}\right) \geq 2f_{p+1}\left(\frac{1}{2}\right)$. Plugging into (E71) gives

$$mf_{p+1}\left(\frac{3}{2m}\right) = \frac{\frac{3}{2}\left(\frac{p+1}{2} - \frac{3}{2m}\right)}{(p+1)!} \prod_{q=1}^{\frac{p-1}{2}} \left[q^2 - \left(\frac{3}{2m}\right)^2 \right], \quad (\text{E72})$$

$$2f_{p+1}\left(\frac{1}{2}\right) = \frac{1\left(\frac{p+1}{2} - \frac{1}{2}\right)}{(p+1)!} \prod_{q=1}^{\frac{p-1}{2}} \left[q^2 - \left(\frac{1}{2}\right)^2 \right]. \quad (\text{E73})$$

Now compare (E72) and (E73) factor by factor. First, $\frac{3}{2} > 1$. Next, note that for $m \geq 3$, we have $\frac{3}{2m} \leq \frac{1}{2}$. Thus, $\frac{p+1}{2} - \frac{3}{2m} \geq \frac{p+1}{2} - \frac{1}{2} > 0$, and, finally,

$q^2 - \left(\frac{3}{2m}\right)^2 \geq q^2 - \left(\frac{1}{2}\right)^2 > 0$. Clearly (E72) is greater than (E73) when $m \geq 3$.

Now consider Claim II. If $\varepsilon = \frac{2}{3m}$, then $m\varepsilon - \lfloor m\varepsilon \rfloor = \frac{2}{3}$, and (E70) reduces to $mf_{p+1}\left(\frac{2}{3m}\right) \geq 2f_{p+1}\left(\frac{2}{3}\right)$. Consider first the $m = 2$ case, for which (E70) reduces to $2f_{p+1}\left(\frac{1}{3}\right) \geq 2f_{p+1}\left(\frac{2}{3}\right)$. From Lemma B.1 of Krzysik,¹⁵ $f_{p+1}(z)$ is symmetric about $z = \frac{1}{2}$, therefore the statement $2f_{p+1}\left(\frac{1}{3}\right) \geq 2f_{p+1}\left(\frac{2}{3}\right)$ must hold with equality. Now consider $m \geq 3$, for which we again make use of (E71). Plugging $\varepsilon = \frac{2}{3m}$ into (E71) we have

$$mf_{p+1}\left(\frac{2}{3m}\right) = \frac{\frac{2}{3}\left(\frac{p+1}{2} - \frac{2}{3m}\right)}{(p+1)!} \prod_{q=1}^{\frac{p-1}{2}} \left[q^2 - \left(\frac{2}{3m}\right)^2 \right]. \quad (\text{E74})$$

Notice that all of the individual factors in (E74) are positive for $m \geq 2$, and, furthermore, that they are all strictly increasing for $m \geq 2$. Since we have $mf_{p+1}\left(\frac{2}{3m}\right) = 2f_{p+1}\left(\frac{2}{3}\right)$ when $m = 2$, it must hold that $mf_{p+1}\left(\frac{2}{3m}\right) > 2f_{p+1}\left(\frac{2}{3}\right)$ for $m > 2$ due to $mf_{p+1}\left(\frac{2}{3m}\right)$ strictly increasing for $m \geq 2$. \square